Supplementary Information (SI) for Chemical Science.
This journal is © The Royal Society of Chemistry 2026

Supporting Information

Minimum Effort, Maximum Effect: Modulating Twisted Intramolecular Charge Transfer for Ultralong Room Temperature Phosphorescence

Wu-Jie Guo, ‡[a] Shirong Yan, ‡[a] Shihao Xu,[a] Tongfei Qi,[a] and Hui-Qing Peng[a]*

[a] State Key Laboratory of Chemical Resource Engineering, Beijing Advanced Innovation Center for Soft Matter Science and Engineering, Beijing University of Chemical Technology, Beijing 100029, China. E-mail: hqpeng@mail.buct.edu.cn

‡ These authors contributed equally to this work.

Contents

1. Materials and Methods

1.1 Materials and Instruments

All reagents were purchased from commercial suppliers and used without further purification. The guest molecules (**SBLs**), 9-julolidinecarboxaldehyde (**QL-CHO**), 4-(azetidin-1-yl)benzaldehyde (**Aze-CHO**), 4-(1-pyrrolidino)benzaldehyde (**Pyr-CHO**), 4-piperidin-1-ylbenzaldehyde (**Pip-CHO**), 4-dimethylaminobenzaldehyde (**N-CHO**), 1-(4-(dimethylamino)phenyl)ethenone (**N-CO**), 4-dimethylaminobenzoic acid (**N-COOH**), and methyl 4-dimethylaminobenzoate (**N-COOMe**) were purchased from commercial suppliers and used after recrystallization with dichloromethane/ *n*-hexane. ^{1}H NMR and ^{13}C NMR spectra were measured on a Bruker Advance III (400 MHz) instrument using chloroform-*d* ($CDCl_3$) and dimethyl sulfoxide-D6 (DMSO-d_6) as the solvent and tetramethylsilane as the internal reference. High resolution mass spectrometry experiments were obtained on Agilent G6540 Q-TOF Mass Spectrometer. UV-vis absorption spectra were measured by a SHIMADZU UV-2600i spectrophotometer. The photoluminescence spectra were measured by a SHIMADZU RF-6000 spectra fluorophotometer, Horiba Fluoremax+ spectrofluorometer and FLS1000 Edinburgh spectrometer. Luminescence decays were measured by time-correlated single photon counting technique using a FLS980 Edinburgh spectrometer and FLS1000 Edinburgh spectrometer with a microsecond flash lamp (μF 900) and pulsed laser. The absolute photoluminescence quantum yields of all doped films were measured on FLS1000 Edinburgh spectrometer with an integrating sphere under ambient conditions. The phosphorescence quantum yields of all doped films were obtained according the reported reference.[1] The excitation wavelengths for photoluminescence spectra and phosphorescence decays were set to 350 nm for **QL-CHO@PVA**, 280 nm for **N-CONMe@PVA** and **N-COOH@PVA**, 260 nm for **N-COOMe@PVA**, and 310 nm for all other samples. EPR analysis was performed on a Bruker E500 Electron Paramagnetic Resonance spectroscopy. The powder X-ray diffraction patterns of doped PVA films were measured by Bruker D2 PHASER Benchtop X-ray diffractometer. Single crystal X-ray diffraction data were collected on a Gemini E X-ray diffraction (Agilent, Oxford) with graphite-monochromator Mo-Kα (λ = 0.71073 Å) at 110 K. Photographs were recorded using a commercial cellphone. The **N-CONMe**, **N-COOH**, **N-COOMe**, and **O-CO** dopped PVA films were irradiated with a 254 nm UV lamp, while the remaining samples were irradiated with a 365 nm UV lamp.

1.2 Preparation of SBL@PVAs Films

The detailed preparation procedure is described using the doped PVA films with a doping concentration of 1 wt% as an example. Firstly, PVA (3.0 g) was added in deionized water (100 mL) and stirred at 90 ℃ until completely dissolved to obtain PVA aqueous solution (30 mg/mL). Then, 1,4-dioxane solution of **SBLs** (3.0 mg/mL, 100 μL) was added into the PVA aqueous solution (30 mg/mL, 1 mL) and the mixed solution were ultrasonicated at 60 ℃ for 0.5 hour for dissolution. Finally, the aqueous solution was drop-coated on quartz glass and the water was removed at 60 ℃ to obtain to obtain doped PVA films (**SBL@PVAs**).

1.3 Theoretical Calculations

The density functional theory (DFT) and time-dependent DFT (TD-DFT) calculations were performed using Gaussian 09, supported by High performance computing platform of BUCT. To justify the choice of functional, representative hybrid functionals with different Hartree-Fock (HF) exact exchange contributions, including B3LYP, PBE0, M06-2X, and CAM-B3LYP, were benchmarked using N-CHO as a representative molecule. Among these functionals, PBE0/Def2-TZVP gave the best agreement with the experimental data (Table S6). Therefore, PBE0/Def2-TZVP was used for the theoretical calculations of the molecular series.

The relaxed potential energy scan of the lowest singlet excited state (S_1) along the dihedral angle φ between the benzene ring and the electron-donating amino group was performed based on the initial optimized molecular structures at ground state (S_0) using PBE0 density function theory at the basis set level of Def2-TZVP. The S_0 potential energy along the dihedral angle φ was obtained by extracting the corresponding S_0 energies from the structures generated in the S_1 relaxed potential energy scan along φ. In this scan, the selected dihedral angle φ was fixed at a given value, while all the other geometrical parameters were optimized at the TD-DFT level. Therefore, the obtained planar and twisted geometries were not manually constructed, but were generated from constrained optimizations along the S_1 twisting coordinate. The planar and twisted geometries of N-CHO, N-CO, and N-COOMe used for the excited-state analysis were representative conformations obtained from the relaxed S_1 potential energy scan. The planar geometry corresponds to the nearly coplanar conformation with $\varphi \approx 0°$, which was used as the LE/planar ICT-like reference structure. For N-CHO and N-CO, $\varphi = 120°$ was selected because it represents a twisted conformation near the rotational barrier region along the S_1 twisting coordinate. For

N-COOMe, φ = 90° was selected because the S_1 energy decreases upon twisting and reaches the TICT-favored region around this angle. Specially, these conformations are constrained minima at fixed φ values along the S_1 potential energy scan, rather than necessarily independent unconstrained local minima on the full S_1 potential energy surface. The excited states of the planar and twisted geometries obtained from the potential energy scan were calculated by single-point energy calculations based on PBE0/ Def2-TZVP level.

Solvent-dependent S_0 to S_1 transition dipole moments (μ) were calculated based on PBE0/ Def2-TZVP level with SMD solvation model. Multiwfn package and VMD software[2-4] is implemented to calculate the hole-electron contributions based on Electron excitation analysis. The components of n orbits are calculated based on Mulliken population analysis (MPA) of Multiwfn package and the reported references.[3, 5, 6] The spin-orbit coupling elements (ξ) were calculated by OCRA.[7-9]

2. Synthesis and Characterization

2.1 Synthesis of N-YT

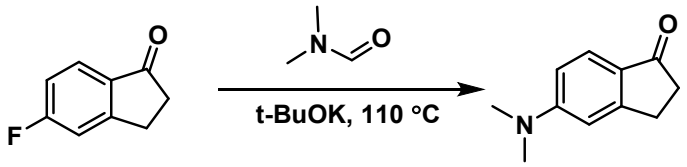

Scheme S1. The synthetic route of **N-YT**.

Synthesis of N-YT: 5-Fluoro-1-indanone (10 mmol, 1.50 g), potassium tert-butoxide (15 mmol, 1.67 g) were added to 100 mL two-neck flask. Under protection of Ar, the anhydrous N, N-dimethylformamide (40 mL) were added and the mixture was stirred for another 24 hours at 110 ℃ under Ar. Then the mixture was extracted with water and dichloromethane. The organic phase was concentrated under vacuum to give the crude product, which was then purified by column chromatography with petroleum ether/ethyl acetate (3:1) to give a yellowish-brown solid (0.12 g, 7%). ^{1}H NMR (400 MHz, $CDCl_3$) δ (ppm) = 7.63 (d, J = 8.7 Hz, 1H), 6.69 (dd, J_1 = 8.7 Hz, J_2 = 2.3 Hz, 1H), 6.60 (s, 1H), 3.08 (s, 6H), 3.05-3.00 (m, 2H), 2.66-2.60 (m, 2H). ^{13}C NMR (101 MHz, $CDCl_3$) δ (ppm) = 204.99, 158.14, 155.13, 125.72, 125.29, 111.79, 106.94, 40.45, 36.54, 26.02. HR-MS: m/z [M+H$^+$] calculated for $C_{11}H_{14}NO$, 176.1075; found, 176.1136.

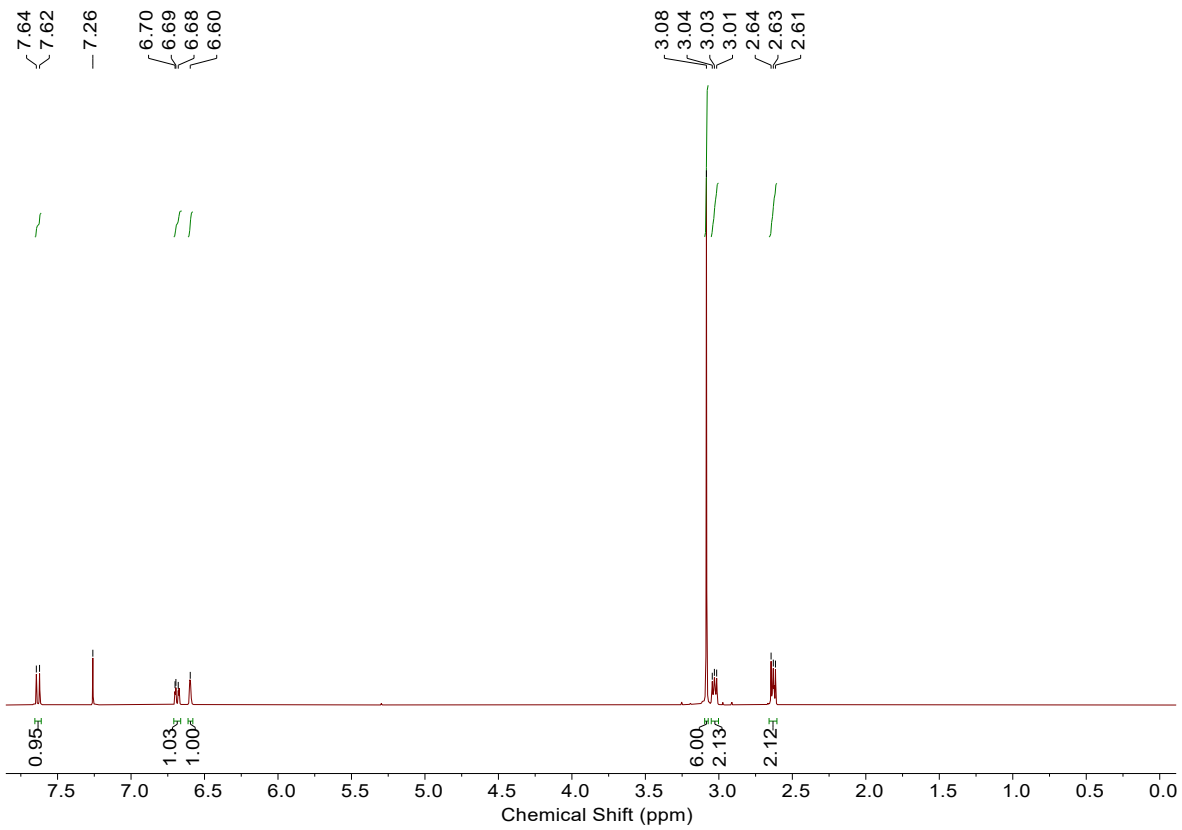

Fig. S1 The ^{1}H NMR spectrum of **N-YT** in $CDCl_3$.

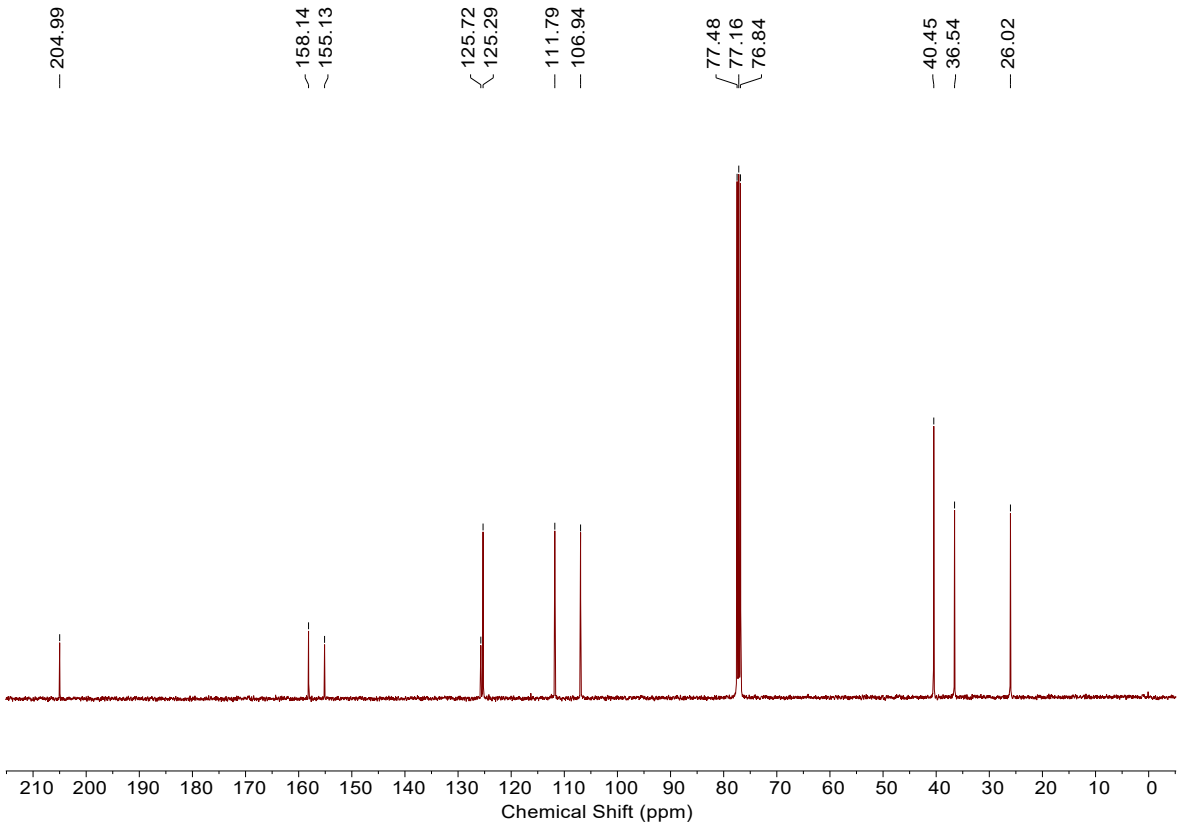

Fig. S2 The ^{13}C NMR spectrum of **N-YT** in $CDCl_3$.

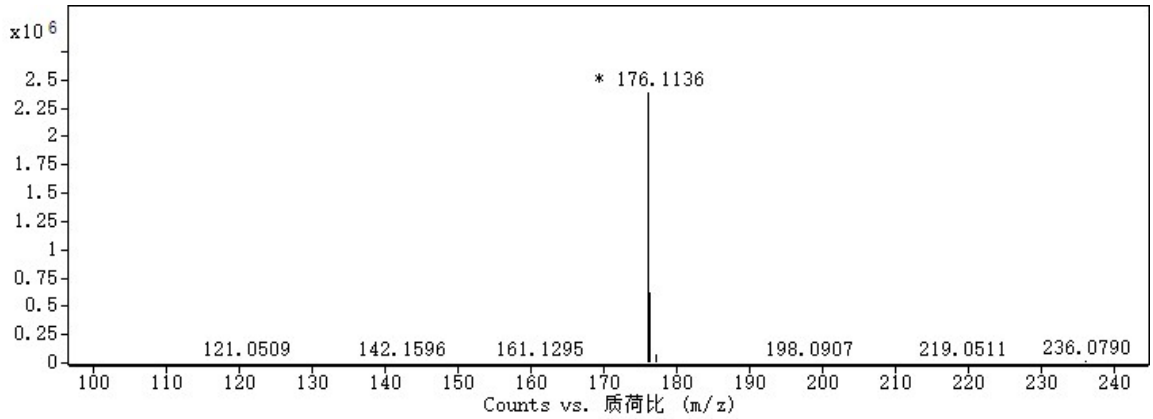

Fig. S3 The HR-MS of **N-YT**.

2.2 Synthesis of N-CONMe

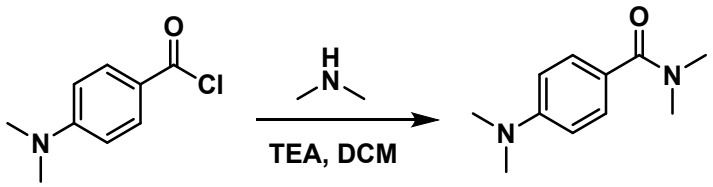

Scheme S2. The synthetic route of **N-CONMe**.

Synthesis of N-CONMe: Dimethylamine of 2.0 M in tetrahydrofuran (30 mmol, 15 mL), (*p*-dimethylamino)benzoyl chloride (10 mmol, 1.83 g), triethylamine (15 mmol, 2.1 mL), and anhydrous dichloromethane (20 mL) were added to flask and stirred for 24 hours at room temperature under the protection of Ar. Then the organic phase was concentrated under vacuum to give the crude product, which was then purified by column chromatography with dichloromethane/methanol (20:1) and recrystallization with dichloromethane/ *n*-hexane to give a white solid (1.56 g, 81%). ^{1}H NMR (400 MHz, $CDCl_3$) δ (ppm) = 7.38 (d, *J* = 8.8 Hz, 2H), 6.67 (d, *J* = 8.8 Hz, 2H), 3.07 (s, 6H), 2.99 (s, 6H). ^{13}C NMR (101 MHz, $CDCl_3$) δ (ppm) = 172.22, 151.38, 129.30, 123.14, 111.12, 40.27, 36.49; at room temperature, signals at 36.49 ppm were broadened out because of rotation of amide. HR-MS: m/z [M+H$^+$] calculated for $C_{11}H_{17}N_2O$, 193.1341; found, 193.1380.

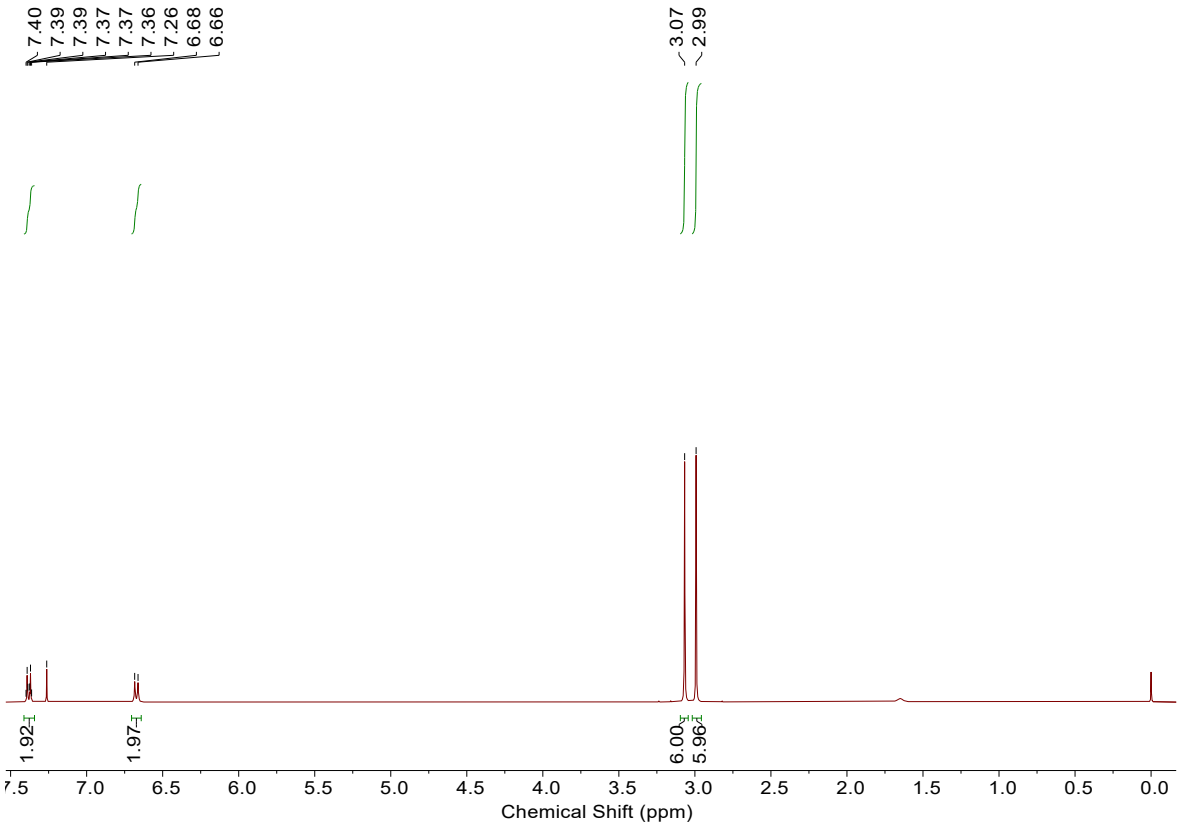

Fig. S4 The ^{1}H NMR spectrum of **N-CONMe** in $CDCl_3$.

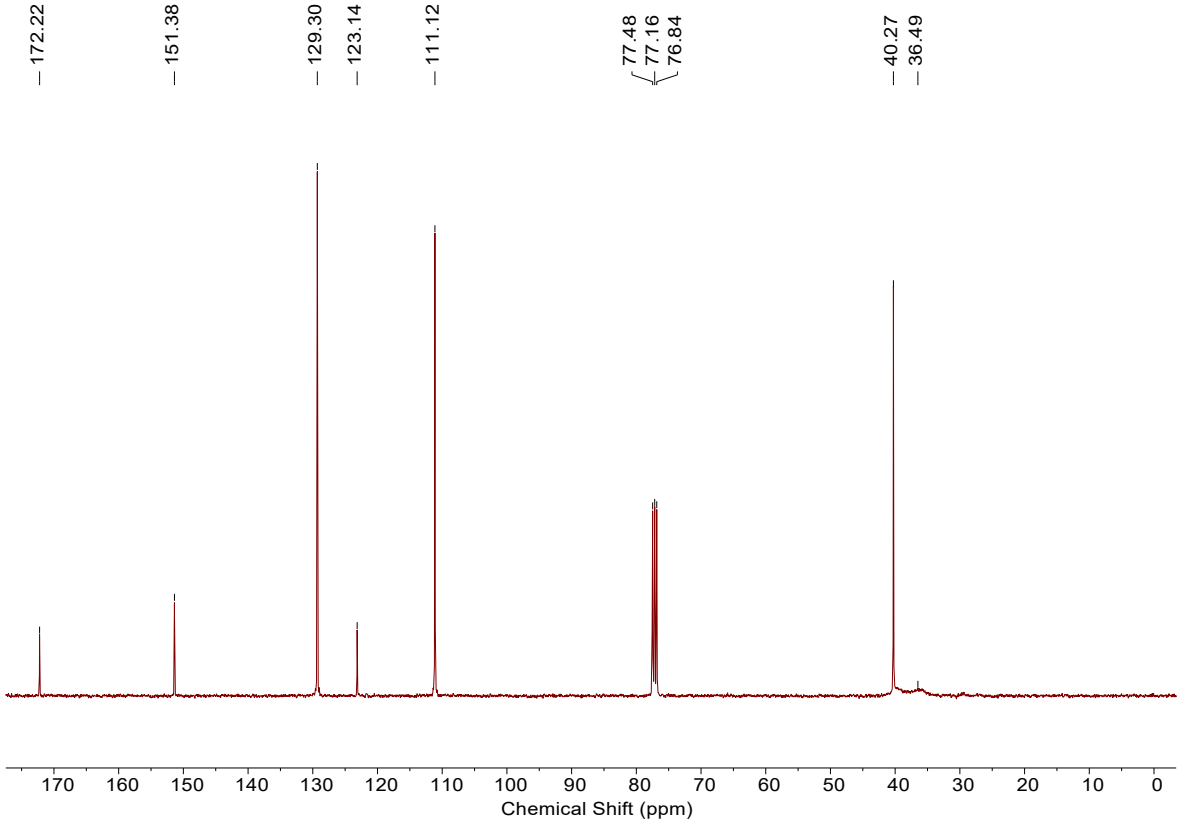

Fig. S5 The ^{13}C NMR spectrum of **N-CONMe** in $CDCl_3$.

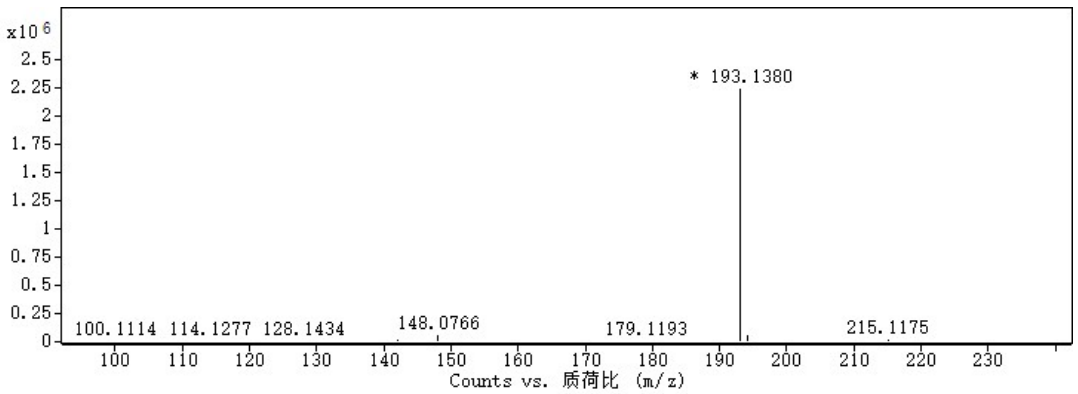

Fig. S6 The HR-MS of **N-CONMe**.

3. Photophysical properties and Theoretical Calculations

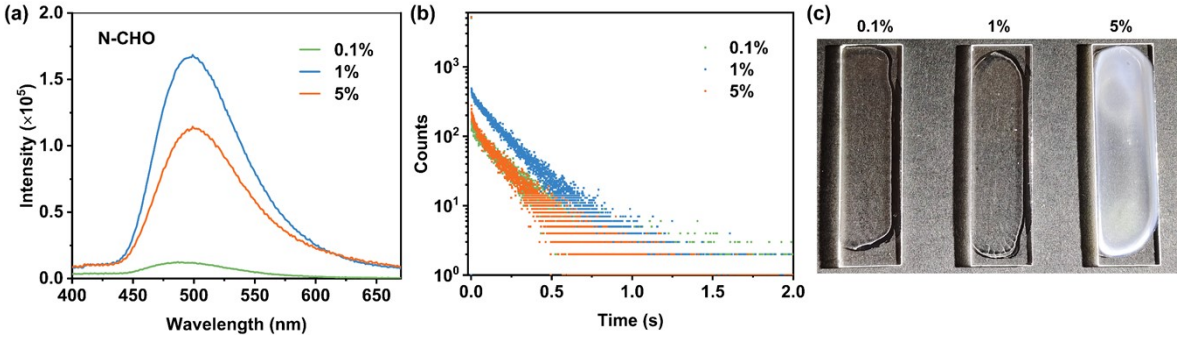

Fig. S7 (a) The phosphorescence spectra, λ_{ex} = 310 nm, EX slit = 2.5 nm, EM slit = 2.5 nm, delay time = 20 ms, (b) the phosphorescence decay curves monitored at 500 nm, λ_{ex} = 310 nm, and (c) the photographs under daylight of **N-CHO** doped films with different doping concentration.

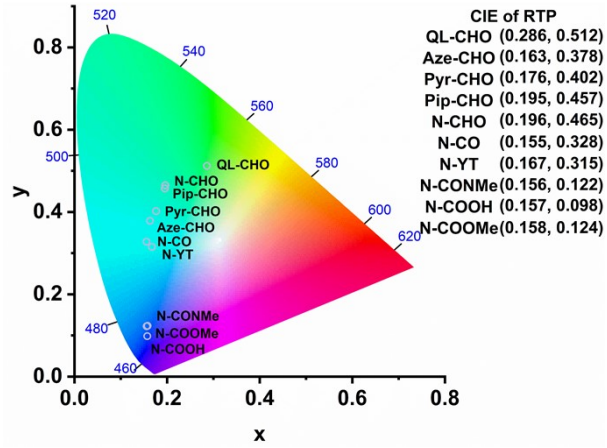

Fig. S8 Phosphorescence CIE 1931 chromaticity diagram of the **SBL@PVAs** with the doped concentration of 1 wt% **SBL** in PVAs

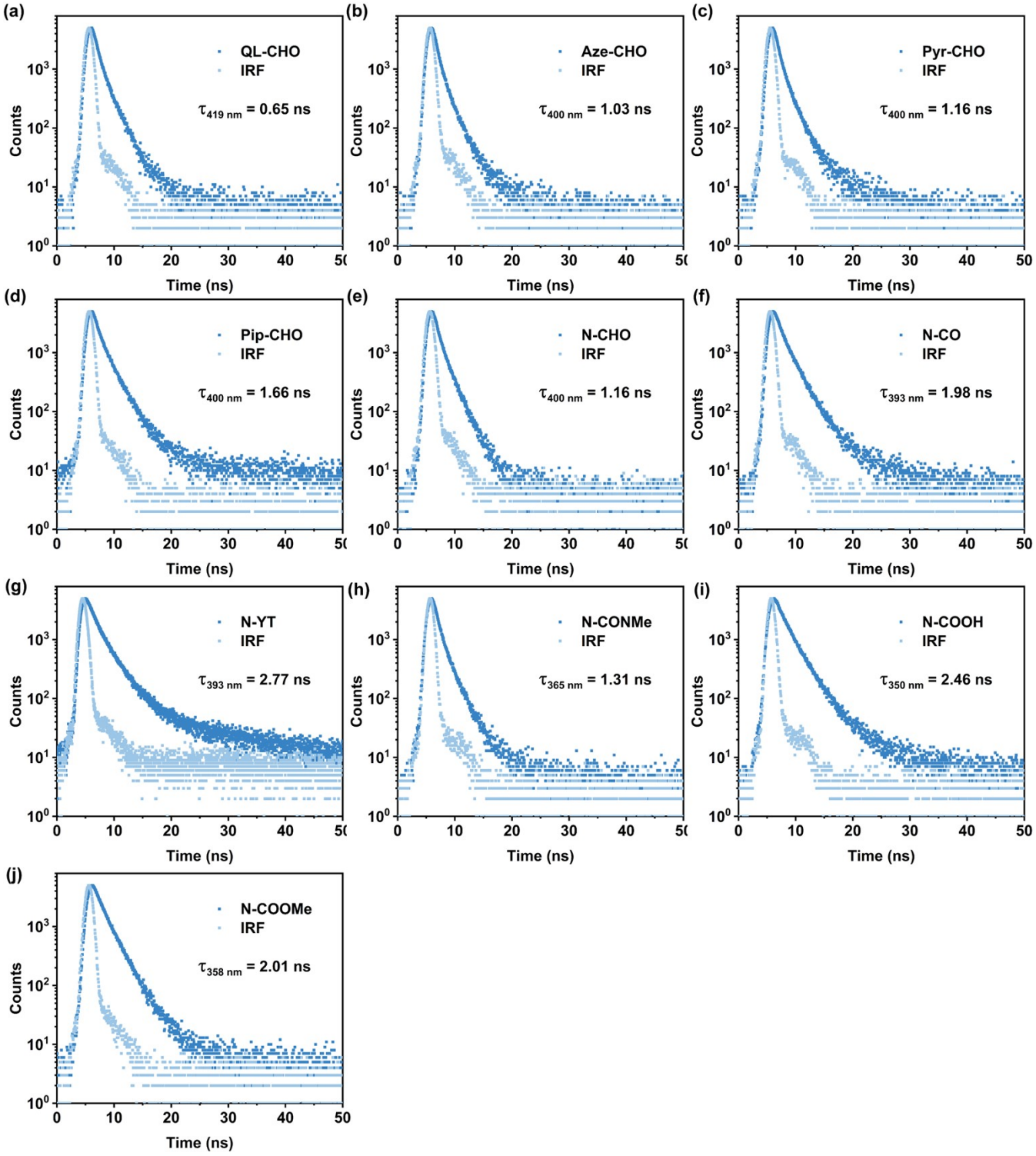

Fig. S9 The fluorescence decay curves of (a) **QL-CHO**, (b) **Aze-CHO**, (c) **Pyr-CHO**, (d) **Pip-CHO**, (e) **N-CHO**, (f) **N-CO**, (g) **N-YT**, (h) **N-CONMe**, (i) **N-COOH**, and (j) **N-COOMe** doped PVA films with doping concentration of 1 wt%.

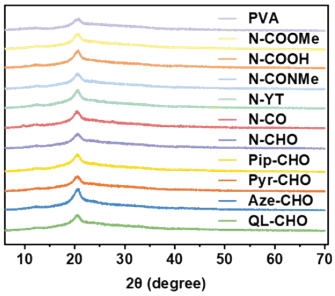

Fig. S10 The powder X-ray diffraction patterns of **SBL@PVAs** and PVA.

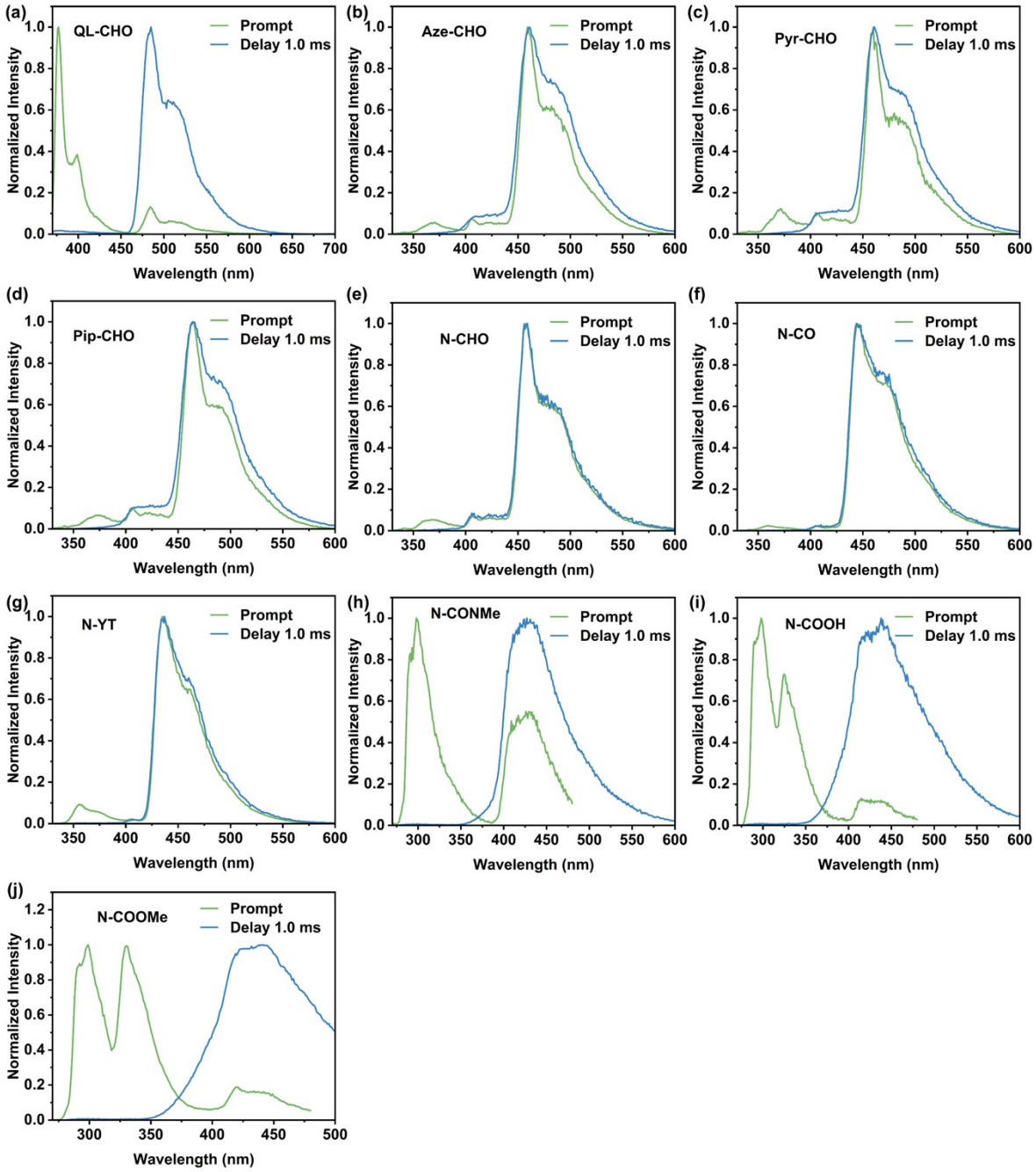

Fig. S11 The prompt and delay emission (delay time: 1.0 ms) spectra of (a) **QL-CHO**, (b) **Aze-CHO**, (c) **Pyr-CHO**, (d) **Pip-CHO**, (e) **N-CHO**, (f) **N-CO**, (g) **N-YT**, (h) **N-CONMe**, (i) **N-COOH**, and (j) **N-COOMe** in dilute 2-methyltetrahydrofuran solution at 77 K, $C = 3\times10^{-4}$ mol/L.

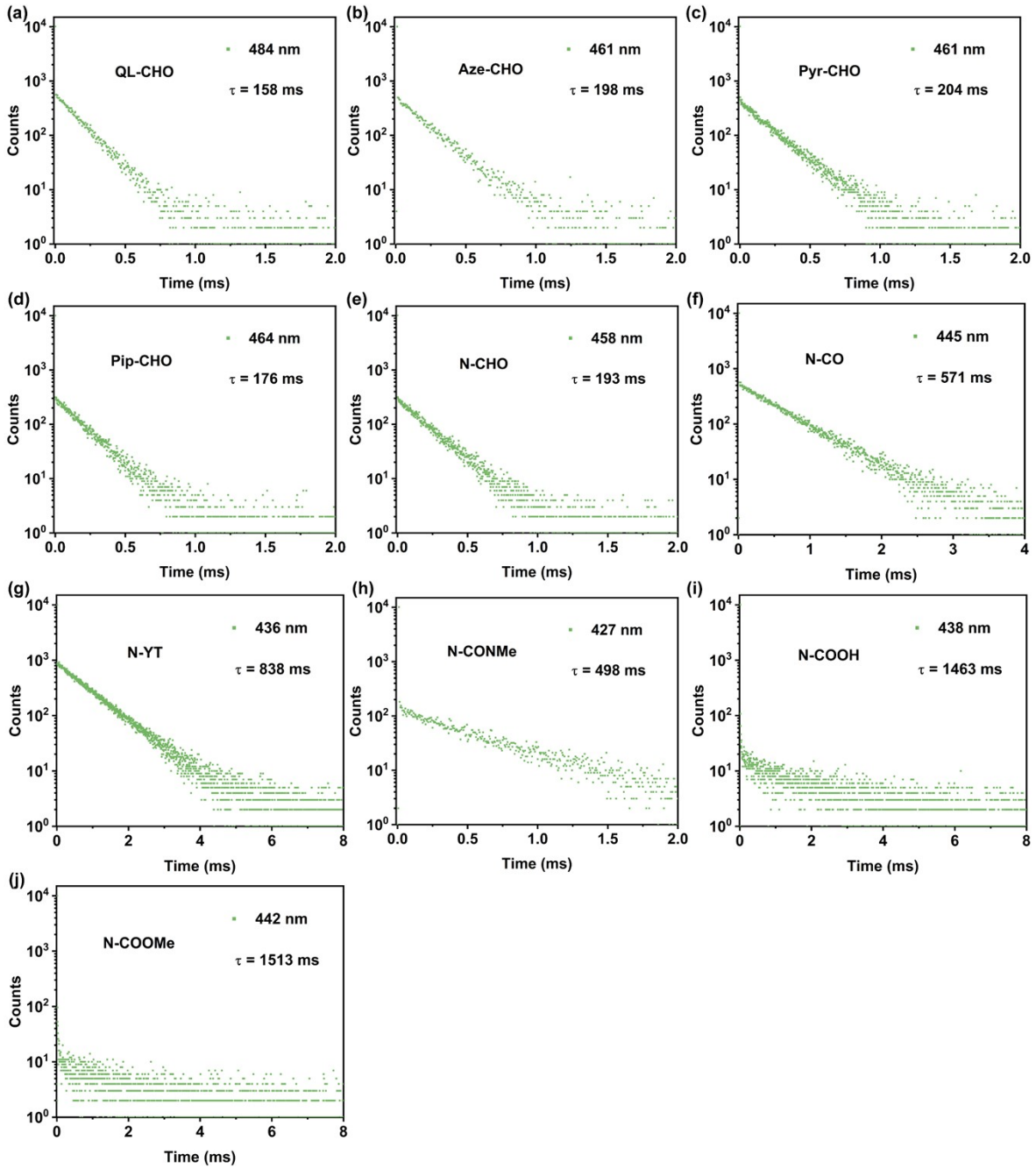

Fig. S12 The phosphorescence decay curves of (a) **QL-CHO**, (b) **Aze-CHO**, (c) **Pyr-CHO**, (d) **Pip-CHO**, (e) **N-CHO**, (f) **N-CO**, (g) **N-YT**, (h) **N-CONMe**, (i) **N-COOH**, and (j) **N-COOMe** in dilute 2-methyltetrahydrofuran solution at 77 K, $C = 3\times10^{-4}$ mol/L.

Table S1 The single crystal data of **N-CHO**, **N-CO**, and **N-COOMe** crystals.

Compound	N-CHO	N-CO	N-COOMe
Empirical formula	$C_9H_{11}NO$	$C_{10}H_{13}NO$	$C_{10}H_{13}NO_2$
Formula weight	149.19	163.21	179.21
Temperature / K	120.25(10)	120.20(10)	120.05(10)
Crystal system	monoclinic	orthorhombic	orthorhombic
Space group	$P2_1/n$	$P2_12_12_1$	$P2_12_12_1$
Unit cell dimensions	a/Å 10.3059(5)	a/Å 5.6298(10)	a/Å 6.0983(5)
	b/Å 7.5527(4)	b/Å 7.9243(18)	b/Å 7.3384(7)
	c/Å 20.5225(12)	c/Å 19.897(4)	c/Å 20.8985(17)
	α/° 90.00	α/° 90.00	α/° 90.00
	β/° 97.542(5)	β/° 90.00	β/° 90.00
	γ/° 90.00	γ/° 90.00	γ/° 90.00
Volume / Å^3	1583.59(15)	887.6(3)	935.24(14)
Z	8	4	4
ρcalc / mg mm^{-3}	1.251	1.221	1.273
μ / mm^{-1}	0.082	0.079	0.089
F(000)	640	352	384
Crystal size / mm^3	0.34 × 0.26 × 0.13	0.35 × 0.34 × 0.01	0.33 × 0.31 × 0.04
2θ range for data collection	6.7 to 52°	6.58 to 51.94°	6.78 to 52°
Index ranges	$-11 \le h \le 12$	$-6 \le h \le 5$	$-5 \le h \le 7$
	$-7 \le k \le 9$	$-6 \le k \le 9$	$-8 \le k \le 6$
	$-23 \le l \le 24$	$-24 \le l \le 24$	$-24 \le l \le 25$
Reflections collected	7724	3542	3820
Independent reflections	3081	1698	1798
Data/restraints/parameters	3081/0/203	1698/0/112	1798/0/122
Goodness-of-fit on F^2	1.047	0.990	1.043
Final R indexes [I>2σ (I)]	$R_1 = 0.0601$	$R_1 = 0.0612$	$R_1 = 0.0492$
	$wR_2 = 0.1133$	$wR_2 = 0.1032$	$wR_2 = 0.0898$
Final R indexes [all data]	$R_1 = 0.1178$	$R_1 = 0.1044$	$R_1 = 0.0670$
	$wR_2 = 0.1485$	$wR_2 = 0.1257$	$wR_2 = 0.1006$
Largest diff. peak/hole / e Å^{-3}	0.197/-0.248	0.148/-0.160	0.153/-0.148
Completeness	0.9971	0.9939	0.9951
CCDC	2519407	2518935	2519406

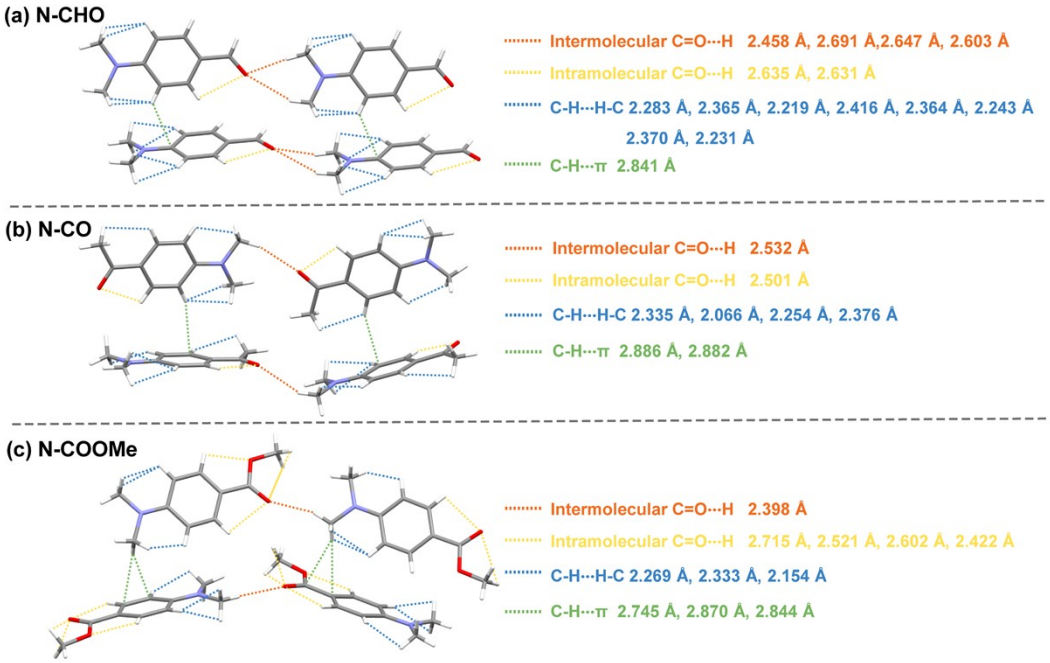

Fig. S13 The molecular stacking and intermolecular/intramolecular interactions of (a) **N-CHO**, (b) **N-CO**, and (c) **N-COOMe** crystals.

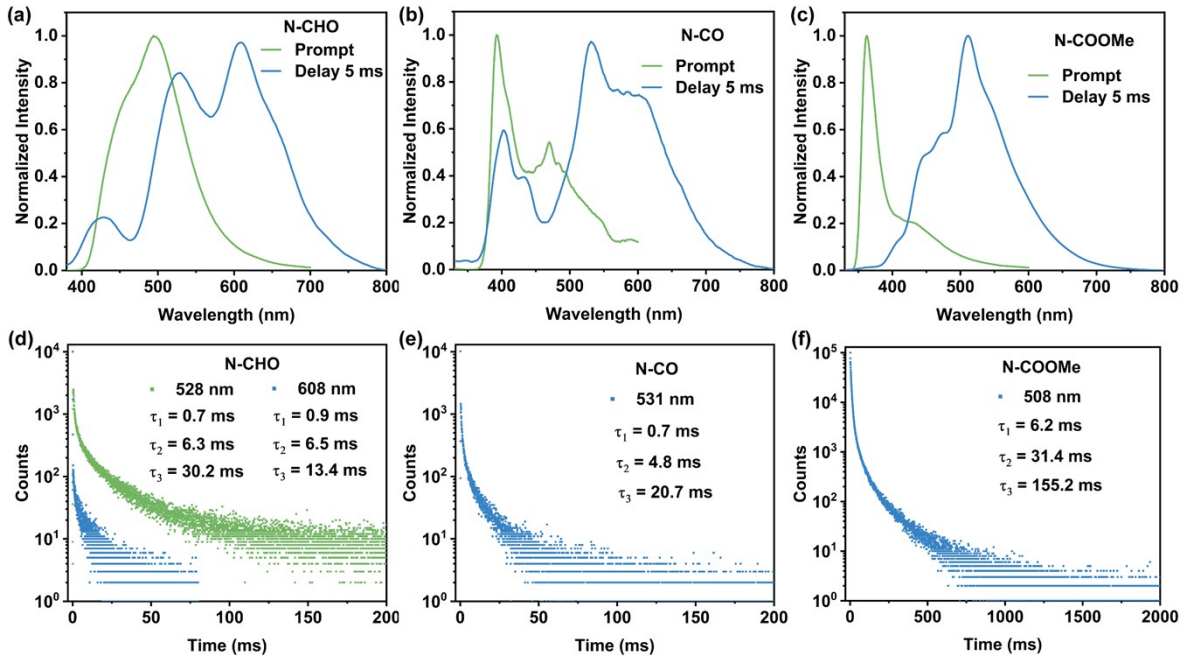

Fig. S14 The prompt and delay emission (delay time: 5.0 ms) spectra of (a) **N-CHO**, (b) **N-CO**, and (c) **N-COOMe** crystals; the phosphorescence decay curves of (d) **N-CHO**, (e) **N-CO**, and (f) **N-COOMe** crystals; λ_{ex} = 310 nm.

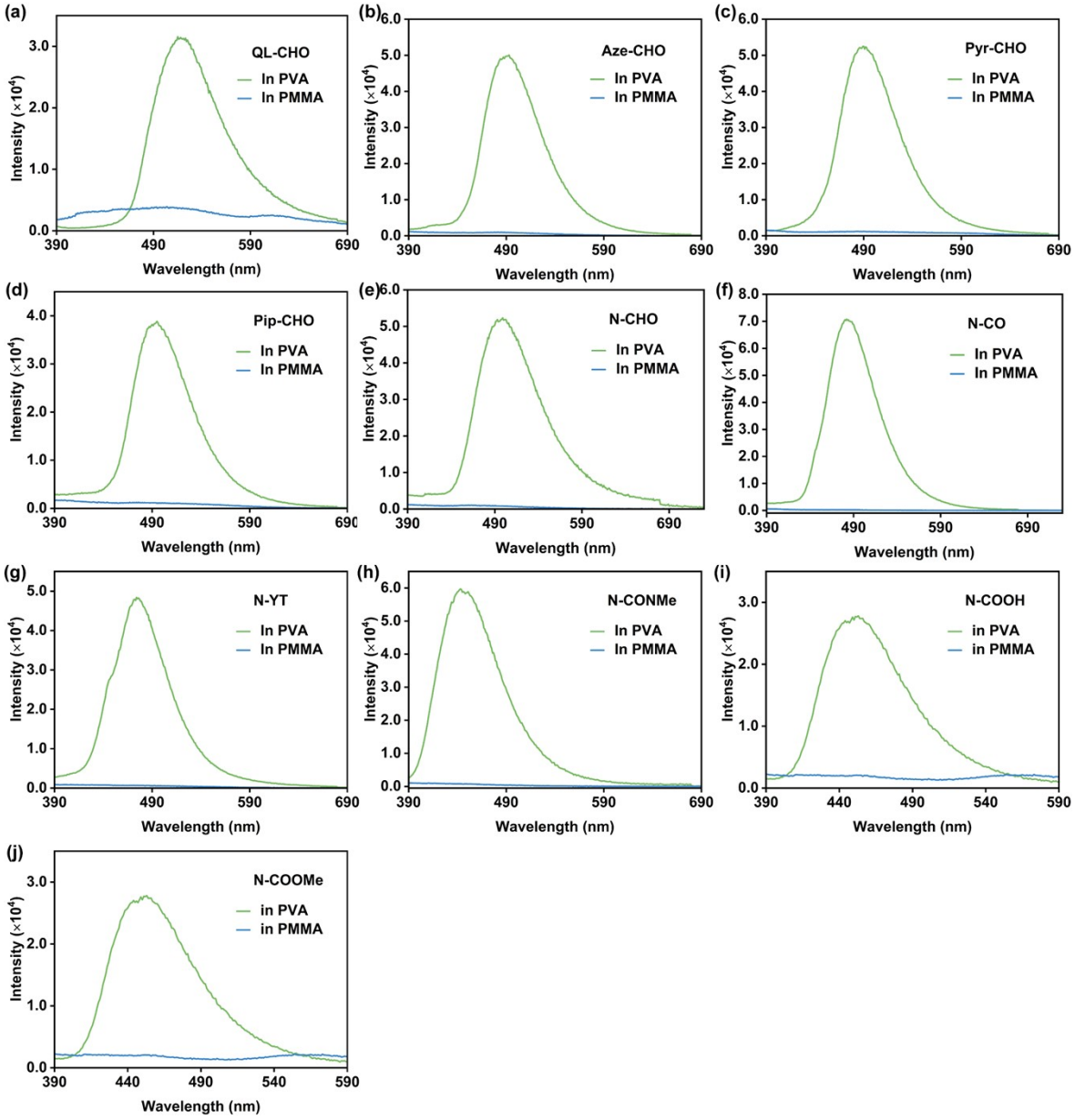

Fig. S15 The phosphorescence spectra of (a) **QL-CHO**, (b) **Aze-CHO**, (c) **Pyr-CHO**, (d) **Pip-CHO**, (e) **N-CHO**, (f) **N-CO**, (g) **N-YT**, (h) **N-CONMe**, (i) **N-COOH**, and (j) **N-COOMe** doped into PVA and PMMA with doping concentration of 1 wt%, delay time = 20 ms.

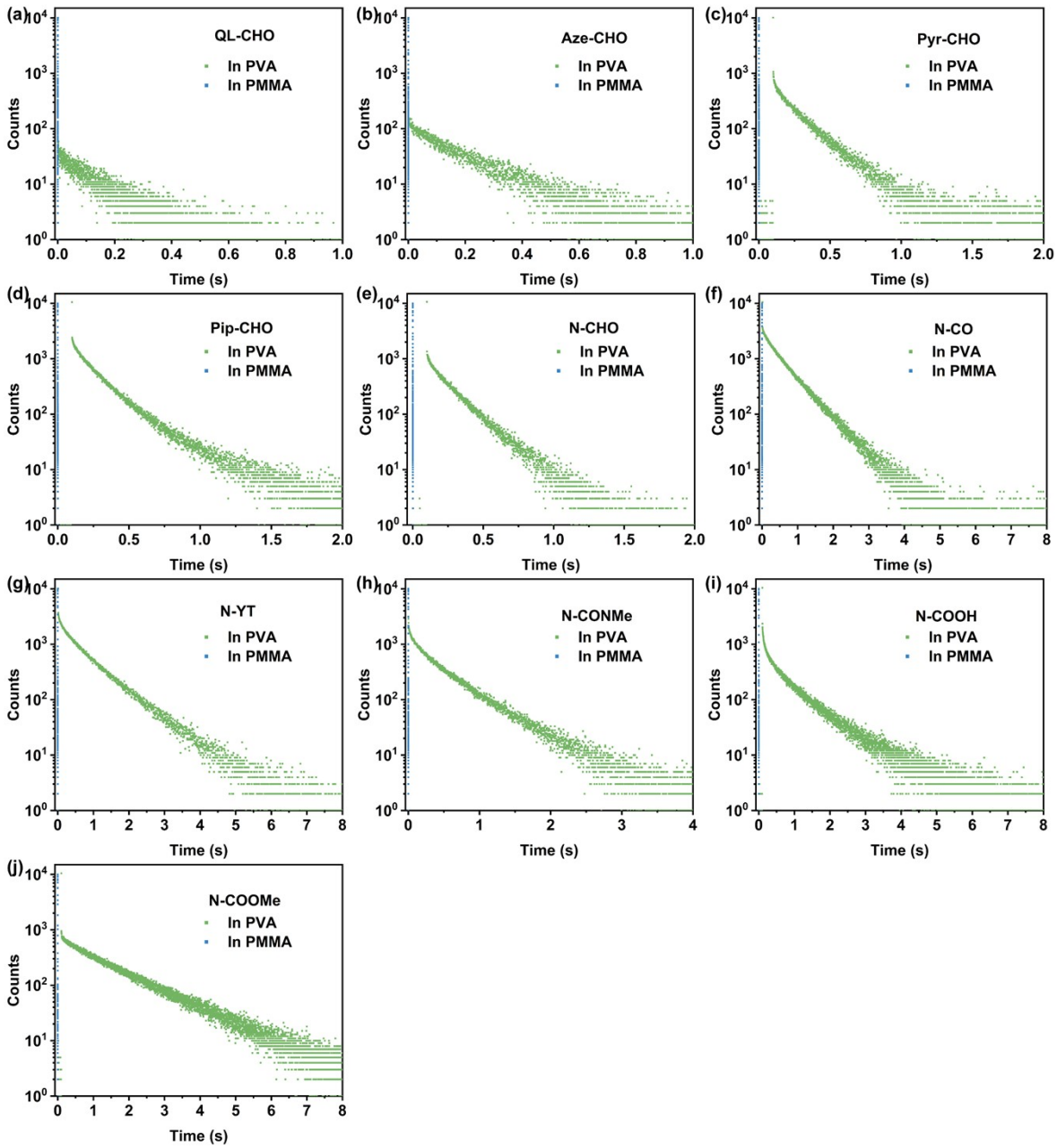

Fig. S16 The phosphorescence decay curves of (a) **QL-CHO**, (b) **Aze-CHO**, (c) **Pyr-CHO**, (d) **Pip-CHO**, (e) **N-CHO**, (f) **N-CO**, (g) **N-YT**, (h) **N-CONMe**, (i) **N-COOH**, and (j) **N-COOMe** doped into PVA and PMMA with doping concentration of 1 wt%.

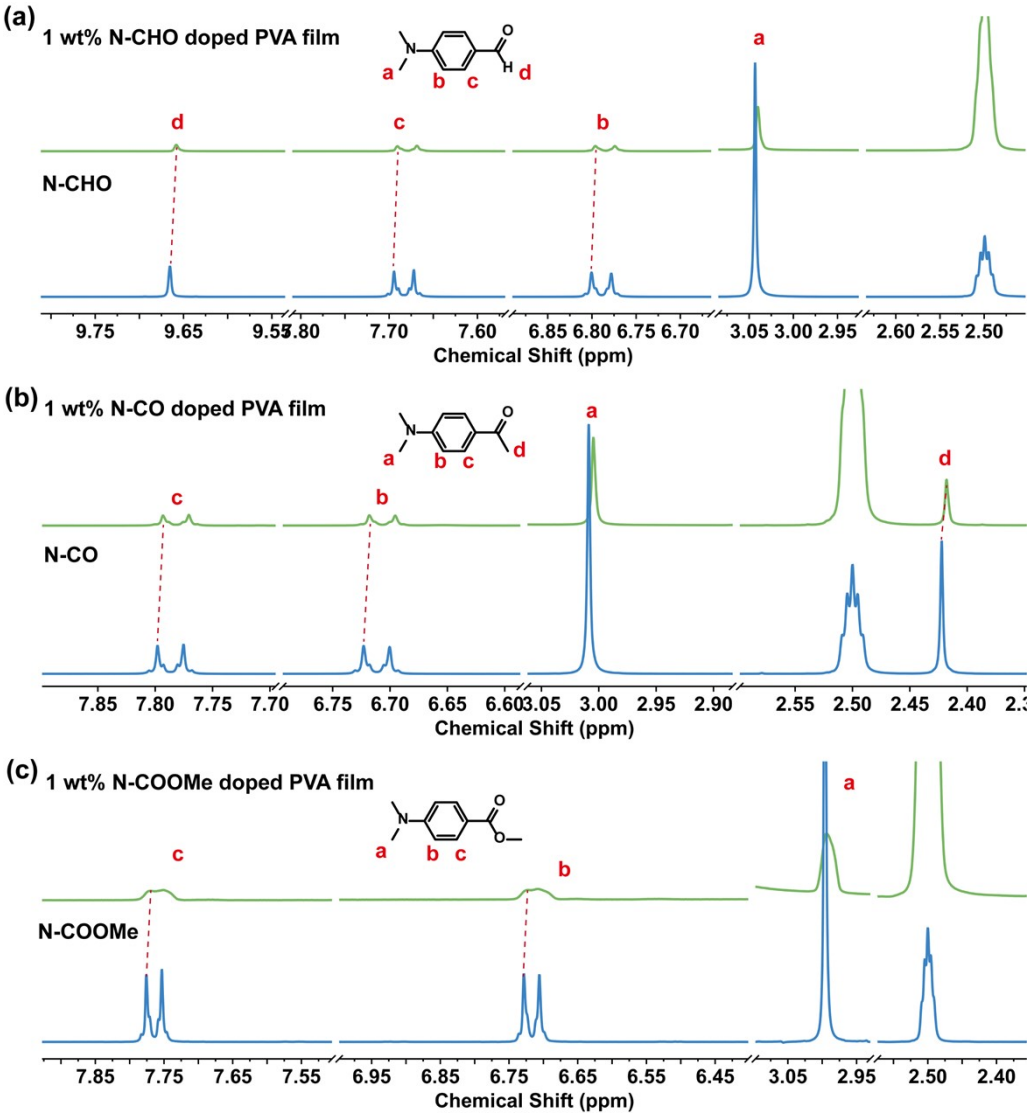

Fig. S17 The ^{1}H NMR spectra of (a) **N-CHO** and **N-CHO** doped PVA film, (b) **N-CO** and **N-CO** doped PVA film, and (c) **N-COOMe** and **N-COOMe** doped PVA film in DMSO-d_6 with doping concentration of 1 wt%.

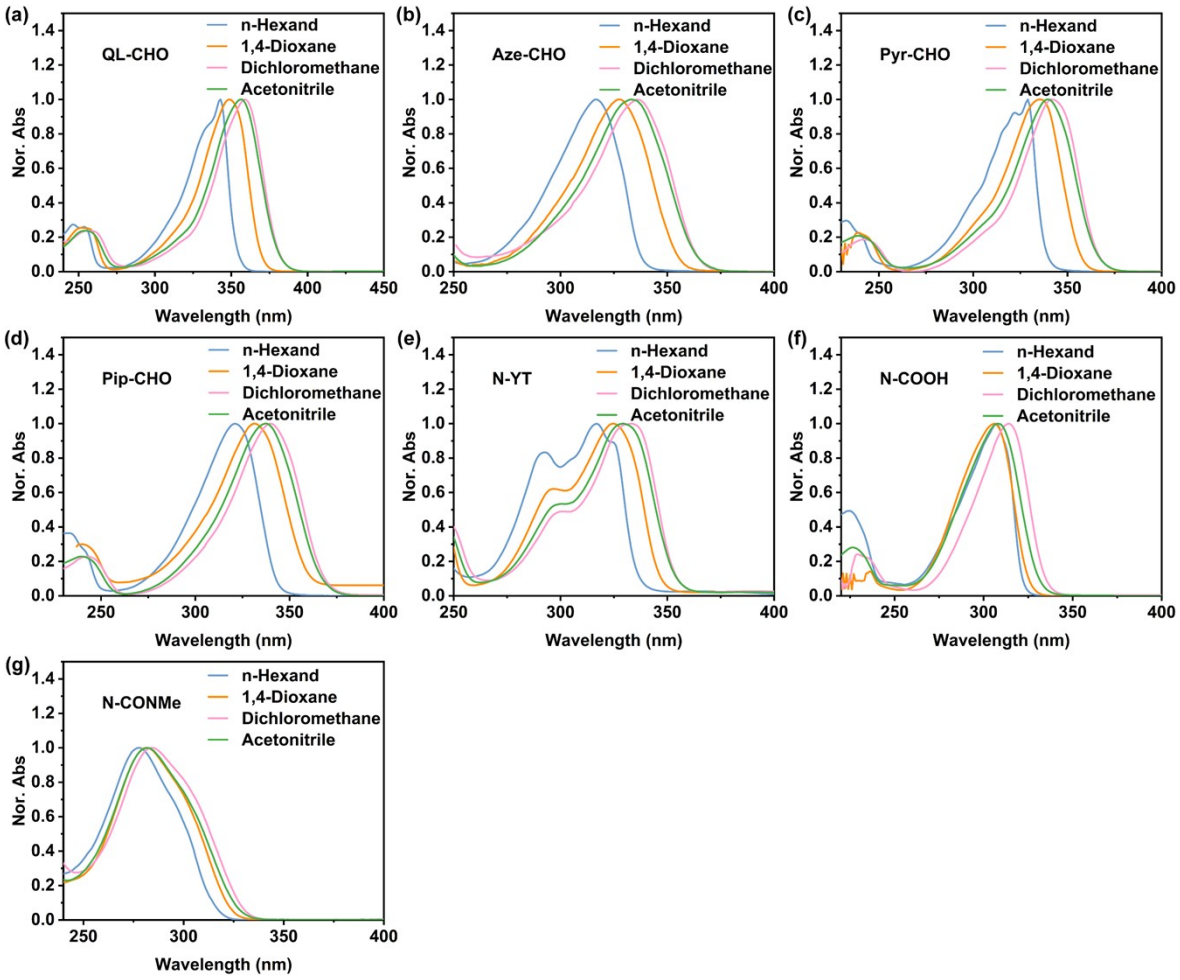

Fig. S18 The absorption spectra of (a) **QL-CHO**, (b) **Aze-CHO**, (c) **Pyr-CHO**, (d) **Pip-CHO**, (e) **N-YT**, (f) **N-COOH**, and (g) **N-CONMe** in different solvents, $C = 5\times10^{-5}$ mol/L.

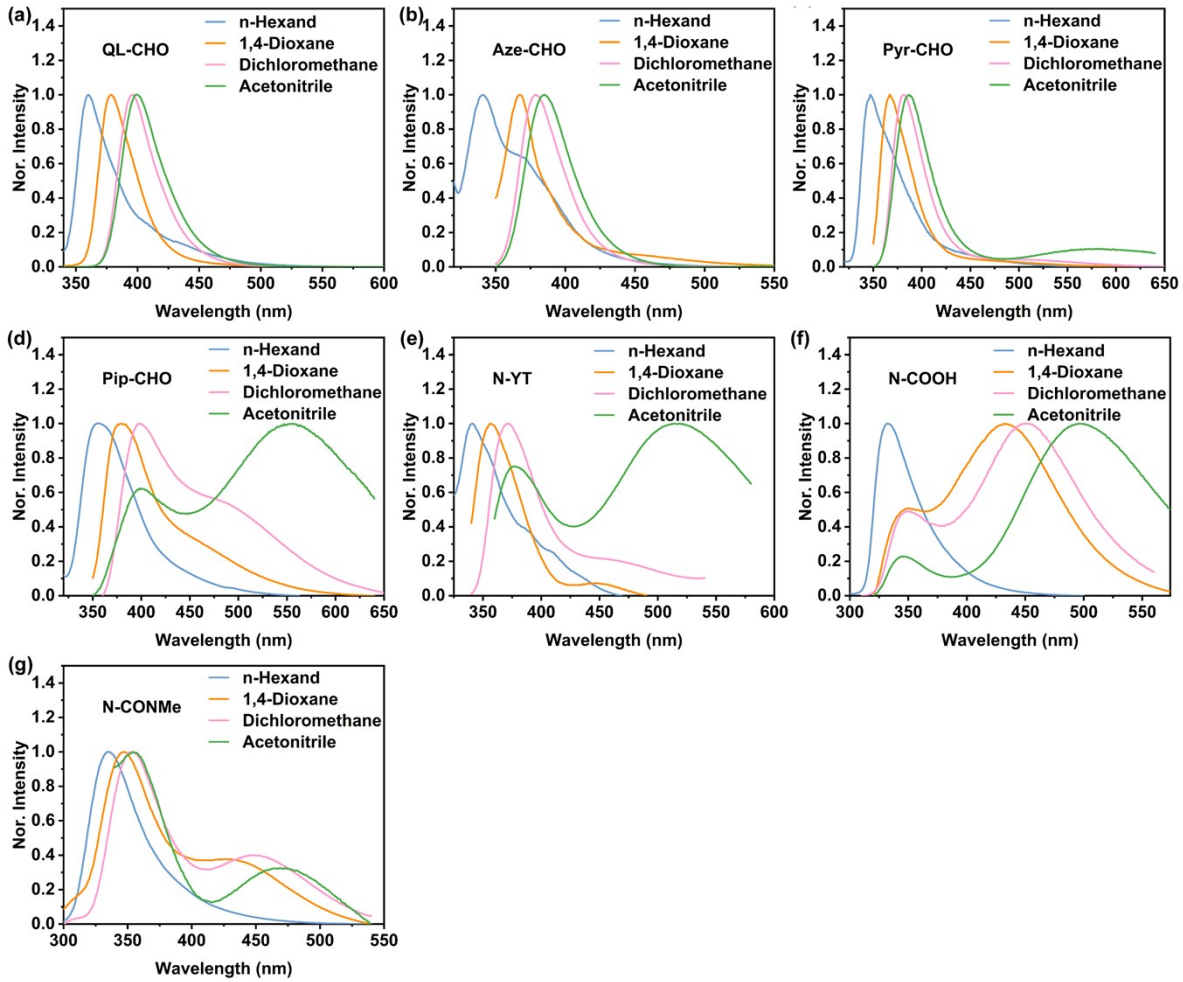

Fig. S19 The fluorescence spectra of (a) **QL-CHO**, (b) **Aze-CHO**, (c) **Pyr-CHO**, (d) **Pip-CHO**, (e) **N-YT**, (f) **N-COOH**, and (g) **N-CONMe** in different solvents, $C = 5\times10^{-5}$ mol/L.

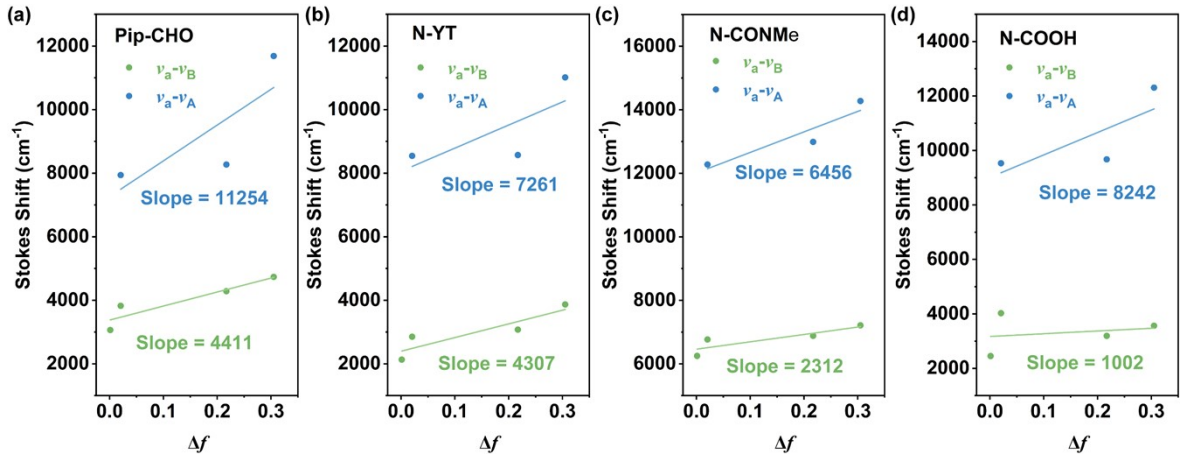

Fig. S20 The relationships between the Stokes shifts and Δ*f* for (a) **Pip-CHO**, (b) **N-YT**, (c) **N-CONMe**, and (d) **N-COOH**.

Table S2 The photophysical properties of ten single benzene molecules in different solvents.

Compound	Solvent	Δf [a]	λ_a [nm]	λ_B [nm]	ν_a-ν_B [cm^{-1}]	λ_A [nm]	ν_a-ν_A [cm^{-1}]
QL-CHO	n-Hexane	0.0012	343	360	1377	--	--
	1,4-Dioxane	0.0206	349	379	2268	--	--
	Dichloromethane	0.217	359	396	2603	--	--
	Acetonitrile	0.305	356	399	3027	--	--
Aze-CHO	n-Hexane	0.0012	316	341	2320	367	4398
	1,4-Dioxane	0.0206	327	367	3333	455	8603
	Dichloromethane	0.217	336	379	3377	--	--
	Acetonitrile	0.305	333	385	4056	--	--
Pyr-CHO	n-Hexane	0.0012	329	347	1577	--	--
	1,4-Dioxane	0.0206	335	367	2603	--	--
	Dichloromethane	0.217	342	381	2993	489	8790
	Acetonitrile	0.305	339	387	3659	583	12346
Pip-CHO	n-Hexane	0.0012	321	356	3063	--	--
	1,4-Dioxane	0.0206	331	379	3827	449	7940
	Dichloromethane	0.217	340	398	4286	473	8270
	Acetonitrile	0.305	337	401	4736	556	11688
N-CHO	n-Hexane	0.0012	324	343	1710	369	3764
	1,4-Dioxane	0.0206	330	359	2448	451	8130
	Dichloromethane	0.217	338	381	3339	479	8709
	Acetonitrile	0.305	336	389	4055	568	12156
N-CO	n-Hexane	0.0012	314	342	2607	371	4893
	1,4-Dioxane	0.0206	322	357	3045	427	7637
	Dichloromethane	0.217	330	375	3636	456	8373
	Acetonitrile	0.305	326	381	4428	530	11807
N-YT	n-Hexane	0.0012	317	340	2134		
	1,4-Dioxane	0.0206	324	357	2853	448	8543
	Dichloromethane	0.217	333	371	3076	466	8571
	Acetonitrile	0.305	329	377	3870	516	11015
N-CONMe	n-Hexane	0.0012	277	335	6250	--	--
	1,4-Dioxane	0.0206	281	347	6769	429	12277
	Dichloromethane	0.217	284	353	6883	450	12989
	Acetonitrile	0.305	282	354	7212	472	14275
N-COOH	n-Hexane	0.0012	307	332	2453	--	--
	1,4-Dioxane	0.0206	306	349	4026	432	9532
	Dichloromethane	0.217	314	349	3194	451	9674
	Acetonitrile	0.305	308	346	3566	496	12306
N-COOMe	n-Hexane	0.0012	299	331	3233	--	--
	1,4-Dioxane	0.0206	307	349	3920	431	9371
	Dichloromethane	0.217	310	355	4089	436	9322
	Acetonitrile	0.305	308	350	3896	490	12059

[a] $\Delta f = \frac{\varepsilon - 1}{2\varepsilon + 1} - \frac{n^2 - 1}{2n^2 + 1}$, where the ε and n are the dielectric constant and refractive index of the solvents, respectively.[10]

Table S3 The dielectric constant and refractive index of the solvents.

Solvents	ε	n
n-Hexane	1.9	1.375
1,4-Dioxane	2.21	1.422
Dichloromethane	8.93	1.424
Acetonitrile	37.5	1.344

Table S4 The S_0 to S_1 transition electric dipole moment μ for **N-CHO**, **N-CO**, and **N-COOMe** in different solvents.

Compound	Solvent	x [a.u.]	y [a.u.]	z [a.u.]	μ [Debye]
N-CHO	n-Hexane	0.0001	0.0000	-0.0433	0.11
	1,4-Dioxane	0.0001	0.0000	-0.0439	0.11
	Dichloromethane	2.9625	0.2946	-0.0002	7.57
	Acetonitrile	3.0784	0.3207	0.0002	7.87
N-CO	n-Hexane	0.0002	0.0000	0.0389	0.10
	1,4-Dioxane	-0.0003	-0.0000	-0.0398	0.10
	Dichloromethane	-2.9211	-0.0828	-0.0000	7.43
	Acetonitrile	-3.0280	-0.0725	0.0000	7.70
N-COOMe	n-Hexane	-2.5364	-0.1735	0.0002	6.46
	1,4-Dioxane	-2.5995	-0.1799	0.0002	6.62
	Dichloromethane	-2.9511	-0.2225	0.0008	7.52
	Acetonitrile	-3.0517	-0.2305	0.0009	7.78

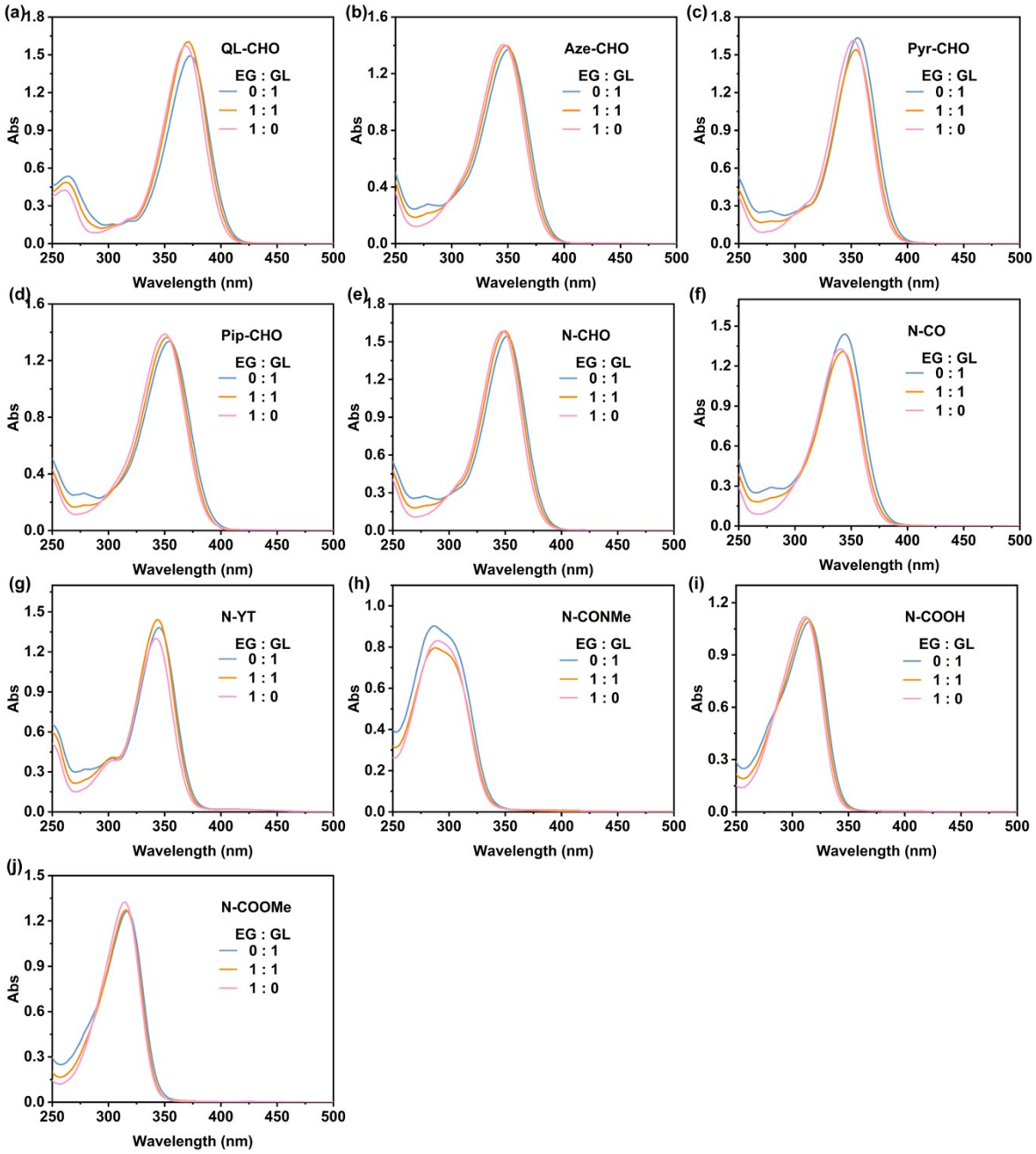

Fig. S21 The absorption spectra of (a) **QL-CHO**, (b) **Aze-CHO**, (c) **Pyr-CHO**, (d) **Pip-CHO**, (e) **N-CHO**, (f) **N-CO**, (g) **N-YT**, (h) **N-CONMe**, (i) **N-COOH**, and (j) **N-COOMe** in solutions with different viscosities (EG: ethylene glycol, GL: glycerol), $C = 5\times10^{-5}$ mol/L.

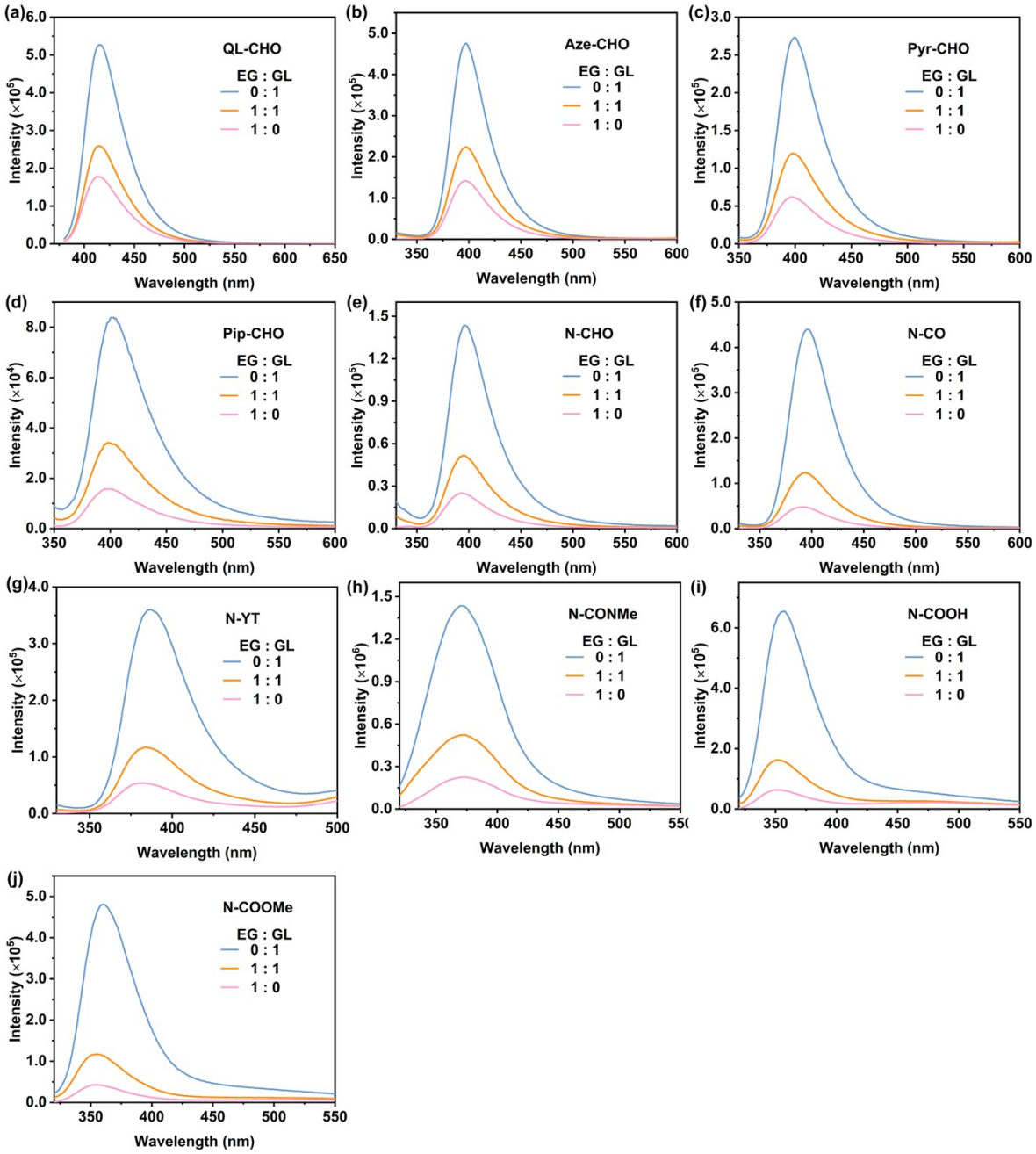

Fig. S22 The fluorescence spectra of (a) **QL-CHO**, (b) **Aze-CHO**, (c) **Pyr-CHO**, (d) **Pip-CHO**, (e) **N-CHO**, (f) **N-CO**, (g) **N-YT**, (h) **N-CONMe**, (i) **N-COOH**, and (j) **N-COOMe** in solutions with different viscosities (EG: ethylene glycol, GL: glycerol), $C = 5\times10^{-5}$ mol/L.

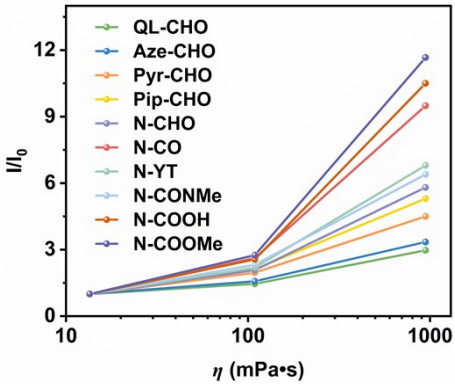

Fig. S23 The relationship between the viscosity (η) and fluorescence intensity ratio (I/I_0), I_0 is the fluorescence intensity of compound in EG, I is the fluorescence intensity of compound in solutions with varying viscosity, η is the viscosity of solution (In 25 ℃, 13.5 mPa•s for EG, 109.0 mPa•s for EG /GL with volume ratio of 1:1, and 945 mPa•s for GL)

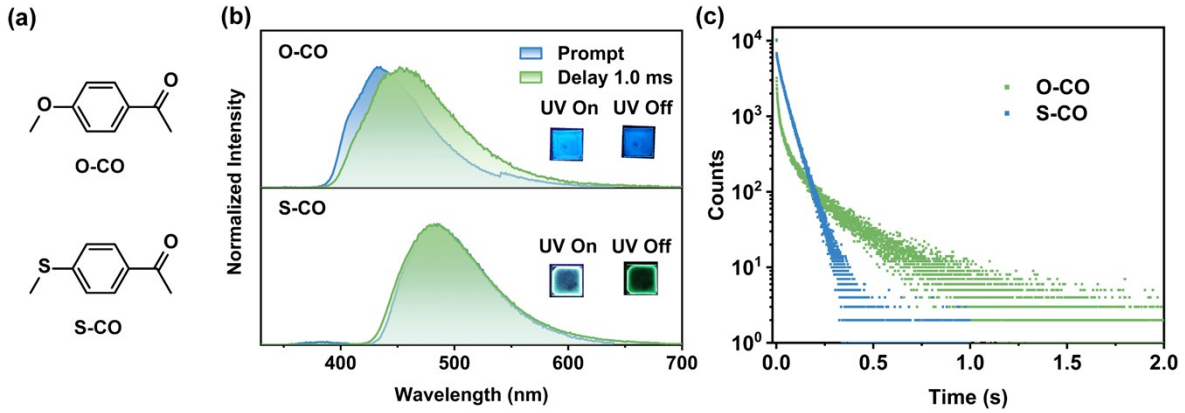

Fig. S24 (a) The chemical structures of **O-CO** and **S-CO**. (b) The normalized prompt and delay emission spectra (delay time = 1.0 ms), insert: the photographs of **O-CO** and **S-CO** doped PVA films before and after removal of the 254 nm or 365 nm UV lamp. (c) The phosphorescence decay curves of **O-CO** and **S-CO** doped PVA films.

Table S5 The photophysical properties of **O-CO** and **S-CO** doped PVA films.

Compound	Φ_{Total} [%]	λ_P [nm]	τ_P [ms]	Φ_P [%]
O-CO	5.47	454	139	2.85
S-CO	56.22	483	46	56.22

Table S6. The calculated wavelengths of S_1 and T_1 using representative hybrid functionals with different Hartree-Fock (HF) exact exchange contributions for **N-CHO**.

Functionals	HF exact exchange contributions	λ_{S1} / nm	λ_{T1} / nm
B3LYP	About 20%	324	431
PBE0	About 25%	383	509
M06-2X	About 54%	320	388
CAM-B3LYP	About 19 for short range and 65% for long range	305	418

Table S7 The potential energy of lowest singlet excited state (S_1) of **SBLs** (except for **QL-CHO** due to the difficult for rotation of the EDG) along with the different dihedral angles (φ) between benzene ring and the EDG, unit: Hartree

φ	Aze-CHO	Pyr-CHO	Pip-CHO	N-CHO	N-CO	N-YT	N-CONMe	N-COOH	N-COOMe
0	-517.0797	-556.3893	-595.6668	-479.0242	-518.3092	-556.3945	-612.9111	-554.2062	-593.4704
15	-517.0804	-556.3885	-595.6655	-479.0243	-518.3098	-556.3947	-612.9113	-554.2078	-593.4737
30	-517.0806	-556.3865	-595.6659	-479.0236	-518.3092	-556.3940	-612.9111	-554.2098	-593.4805
45	-517.0794	-556.3842	-595.6668	-479.0230	-518.3087	-556.3934	-612.9110	-554.2279	-593.4887
60	-517.0770	-556.3824	-595.6665	-479.0220	-518.3078	-556.3927	-612.9109	-554.2343	-593.4948
75	-517.0738	-556.3800	-595.6648	-479.0200	-518.3059	-556.3911	-612.9098	-554.2374	-593.4976
90	-517.0709	-556.3775	-595.6626	-479.0177	-518.3037	-556.3893	-612.9084	-554.2382	-593.4984
105	-517.069	-556.376	-595.6612	-479.0162	-518.3023	-556.3882	-612.9077	-554.2375	-593.4977
120	-517.0685	-556.3758	-595.6610	-479.0160	-518.3021	-556.3881	-612.9076	-554.2351	-593.4954
135	-517.0687	-556.3766	-595.6623	479.0174	-518.3034	-556.3890	-612.9082	-554.2304	-593.4910
150	-517.0806	-556.3880	-595.6652	-479.0237	-518.3063	-556.3914	-612.9097	-554.2239	-593.4847
165	-517.0804	-556.3892	-595.6668	-479.0243	-518.3083	-556.3931	-612.9109	-554.2159	-593.4771
180	-517.0797	-556.3893	-595.6664	-479.0242	-518.3096	-556.3945	-612.9110	-554.2076	-593.4690

Table S8 The potential energy of lowest singlet excited state (S_0) of **SBLs** (except for **QL-CHO** due to the difficult for rotation of the EDG) along with the different dihedral angles (φ) between benzene ring and the EDG, unit: Hartree

φ	Aze-CHO	Pyr-CHO	Pip-CHO	N-CHO	N-CO	N-YT	N-CONMe	N-COOH	N-COOMe
0	-517.1991	-556.5087	-595.7840	-479.1433	-518.4265	-556.5154	-612.9816	-554.3651	-593.6214
15	-517.1991	-556.5076	-595.7835	-479.1429	-518.4245	-556.5150	-612.9840	-554.3598	-593.6020
30	-517.1990	-556.5050	-595.7842	-479.1417	-518.4235	-556.5141	-612.9831	-554.3583	-593.5839
45	-517.1973	-556.5019	-595.7844	-479.1404	-518.4223	-556.5129	-612.9813	-554.3220	-593.5843
60	-517.1941	-556.4992	-595.7833	-479.1386	-518.4206	-556.5113	-612.9796	-554.3284	-593.5907
75	-517.1899	-556.4959	-595.7807	-479.1357	-518.4178	-556.5085	-612.9768	-554.3352	-593.5977
90	-517.1859	-556.4925	-595.7777	-479.1326	-518.4149	-556.5055	-612.9735	-554.3377	-593.6002
105	-517.1833	-556.4905	-595.7758	-479.1306	-518.4130	-556.5036	-612.9714	-554.3358	-593.5979
120	-517.1823	-556.4901	-595.7755	-479.1303	-518.4127	-556.5033	-612.9710	-554.3309	-593.5929
135	-517.1826	-556.4913	-595.7774	-479.1322	-518.4145	-556.5050	-612.9728	-554.3262	-593.5883
150	-517.1989	-556.5066	-595.7816	-479.1416	-518.4189	-556.5094	-612.9770	-554.3214	-593.5836
165	-517.1992	-556.5084	-595.7840	-479.1429	-518.4218	-556.5122	-612.9804	-554.3184	-593.5806
180	-517.1991	-556.5087	-595.7841	-479.1433	-518.4248	-556.5155	-612.9804	-554.3178	-593.5802

The energy barrier (E_{EB}) with rotation of the EDG was calculated according to the following formula:

$$E_{EB} = (E_{PE} - E_{PE0}) \times 27.21$$

where E_{PE} is the potential energy of S_1 or S_0 with different φ and E_{PE0} is the potential energy of S_1 or S_0 with φ = 0.

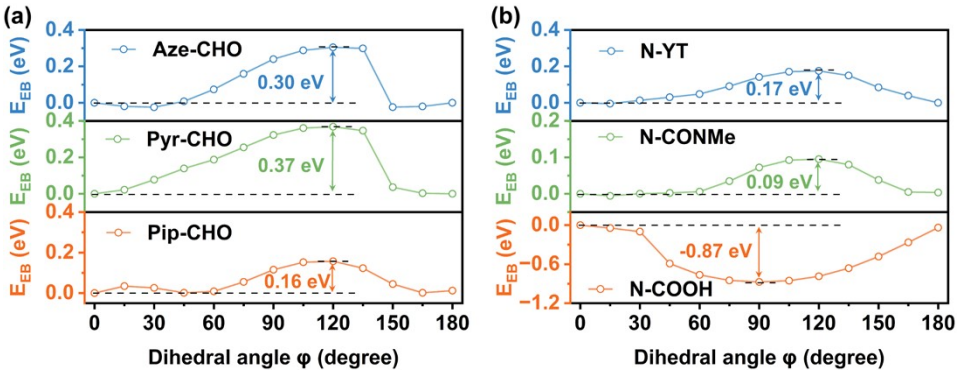

Fig. S25 (a) The E_{EB} of the S_1 for **Aze-CHO** (top), **Pyr-CHO** (middle), and **Pip-CHO** (bottom) with different φ between benzene ring and the EDG. (b) The E_{EB} of the S_1 for **N-YT** (top), **N-CONMe** (middle), and **N-COOH** (bottom) with different φ between benzene ring and the EDG.

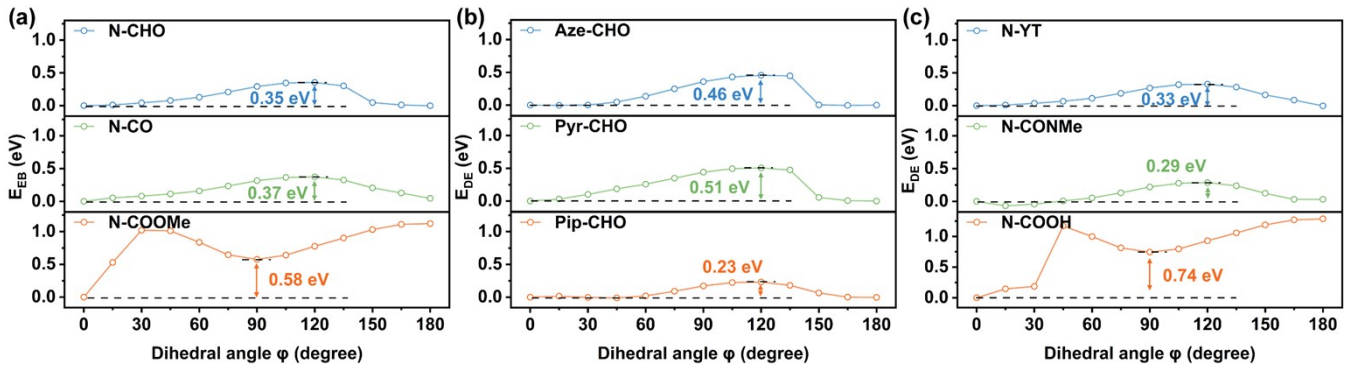

Fig. S26 (a) The E_{EB} of the S_0 for **N-CHO** (top), **N-CO** (middle), and **N-COOMe** (bottom) with different φ between benzene ring and the EDG. (b) The E_{EB} of the S_0 for **Aze-CHO** (top), **Pyr-CHO** (middle), and **Pip-CHO** (bottom) with different φ between benzene ring and the EDG. (c) The E_{EB} of the S_0 for **N-YT** (top), **N-CONMe** (middle), and **N-COOH** (bottom) with different φ between benzene ring and the EDG.

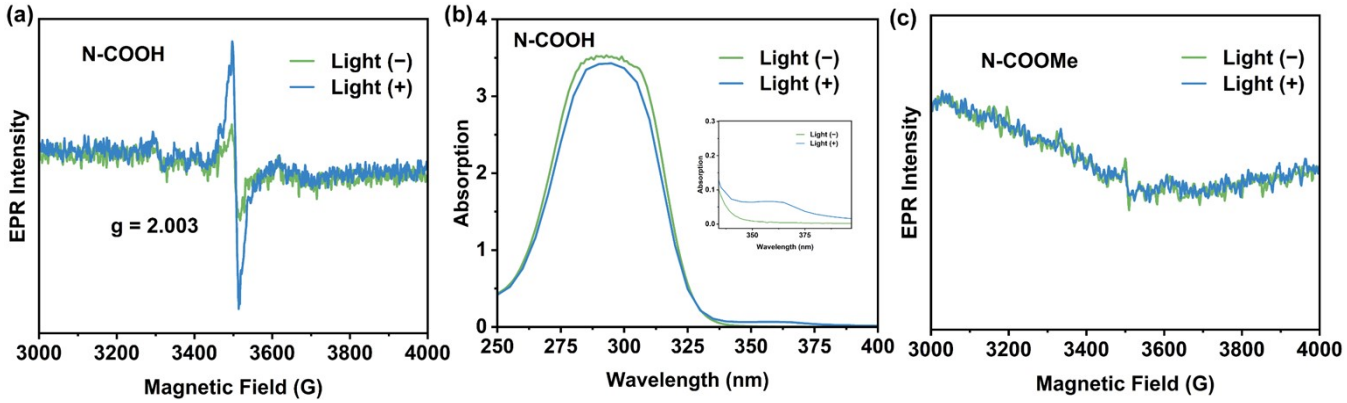

Fig. S27 (a) The EPR spectra before and after irradiation of Xe lamp and (b) the absorption spectra before and after irradiation of 254 nm UV lamp for **N-COOH** doped film with the doped concentration of 1 wt%. (c) The EPR spectra before and after irradiation of Xe lamp for **N-COOMe** doped film with the doped concentration of 1 wt%.

Table S9 The Hammett σ⁻ constant of EWGs[11], dipole moment and LUMO energy of S_0.

	Hammett σ⁻ constant of EWG	Dipole moment [Debye]	LUMO [eV]
N-CHO	1.126	6.54	-1.20
N-CO	0.874	5.76	-1.01
N-COOMe	0.636	4.44	-0.71

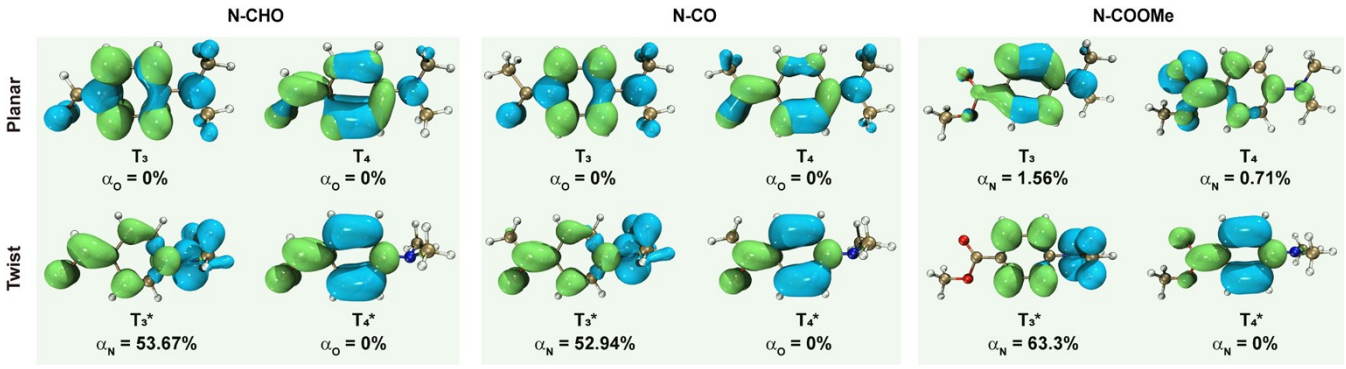

Fig. S28 The hole-electron analysis of **N-CHO** (left), **N-CO** (middle), and **N-COOMe** (right) for their T_3, and T_4 excited states in planar geometries, as well as the T_3*, and T_4* excited states in twisted geometries, with the corresponding proportions of n orbitals (α).

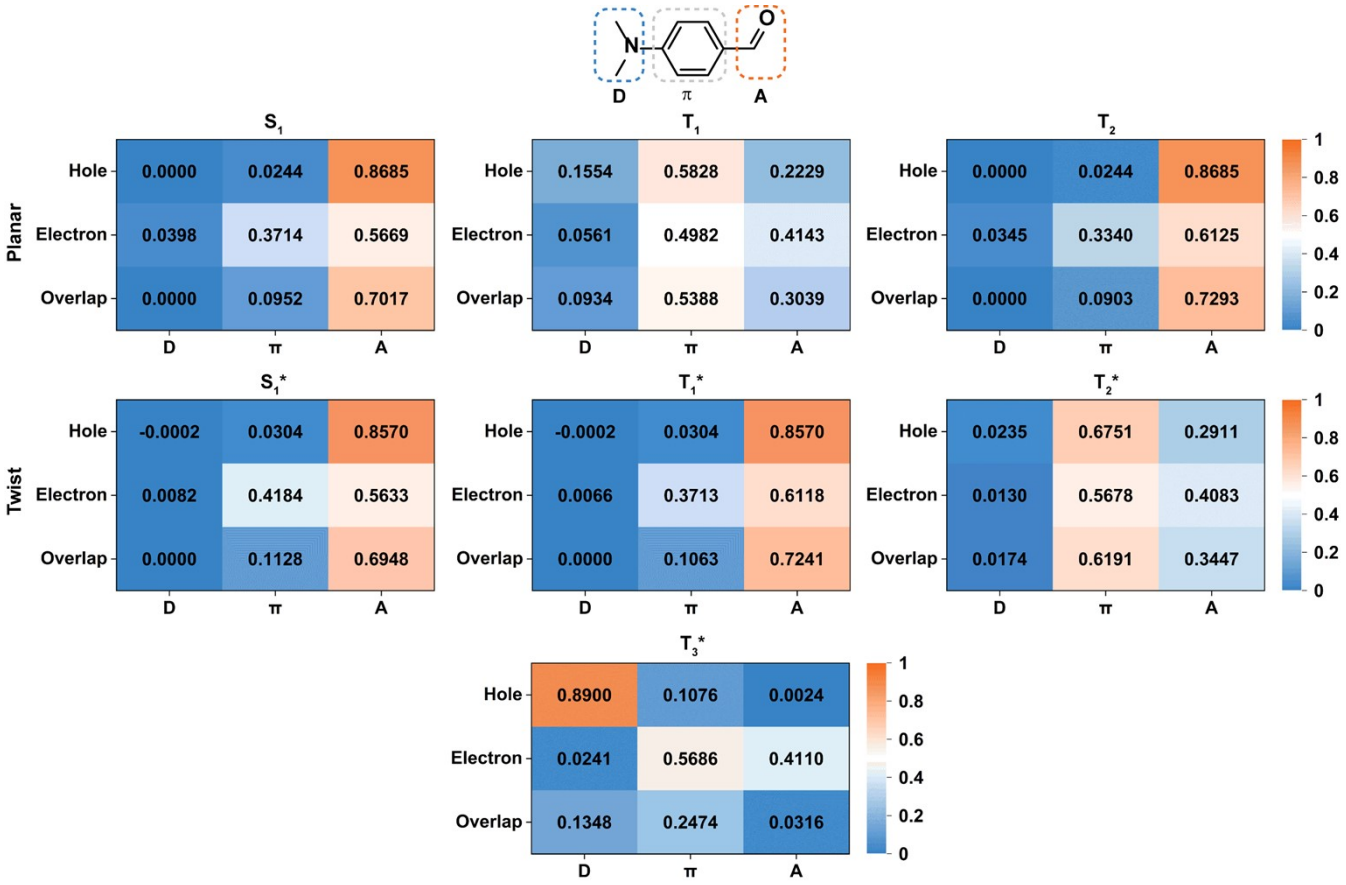

Fig. S29 The heat map of electron and hole contributions from different fragments (D, π, and A) of different excited states in the planar and twisted geometries of **N-CHO**.

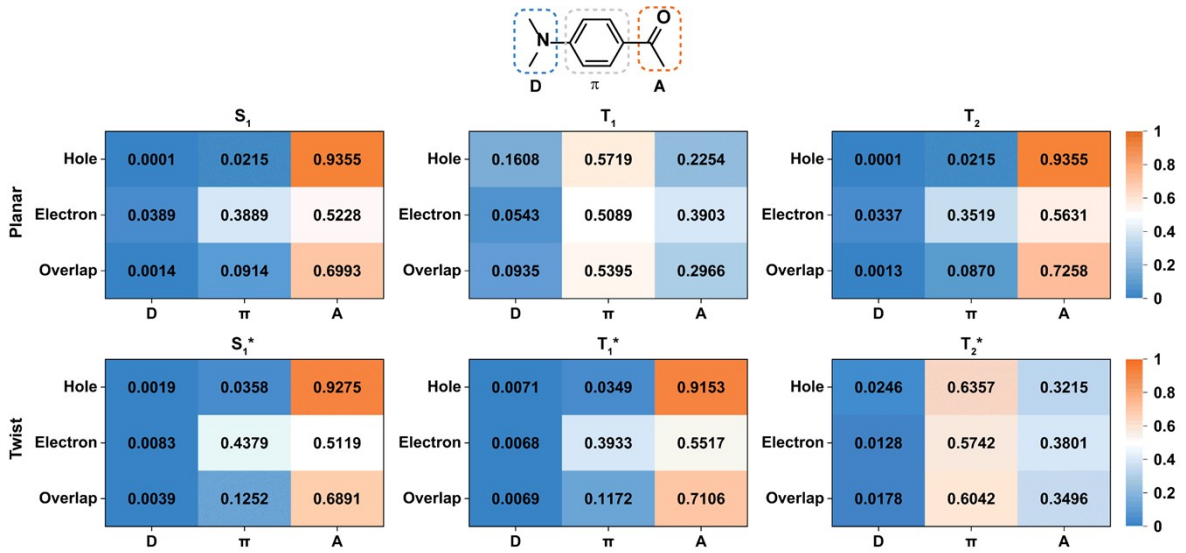

Fig. S30 The heat map of electron and hole contributions from different fragments (D, π, and A) of different excited states in the planar and twisted geometries of **N-CO**.

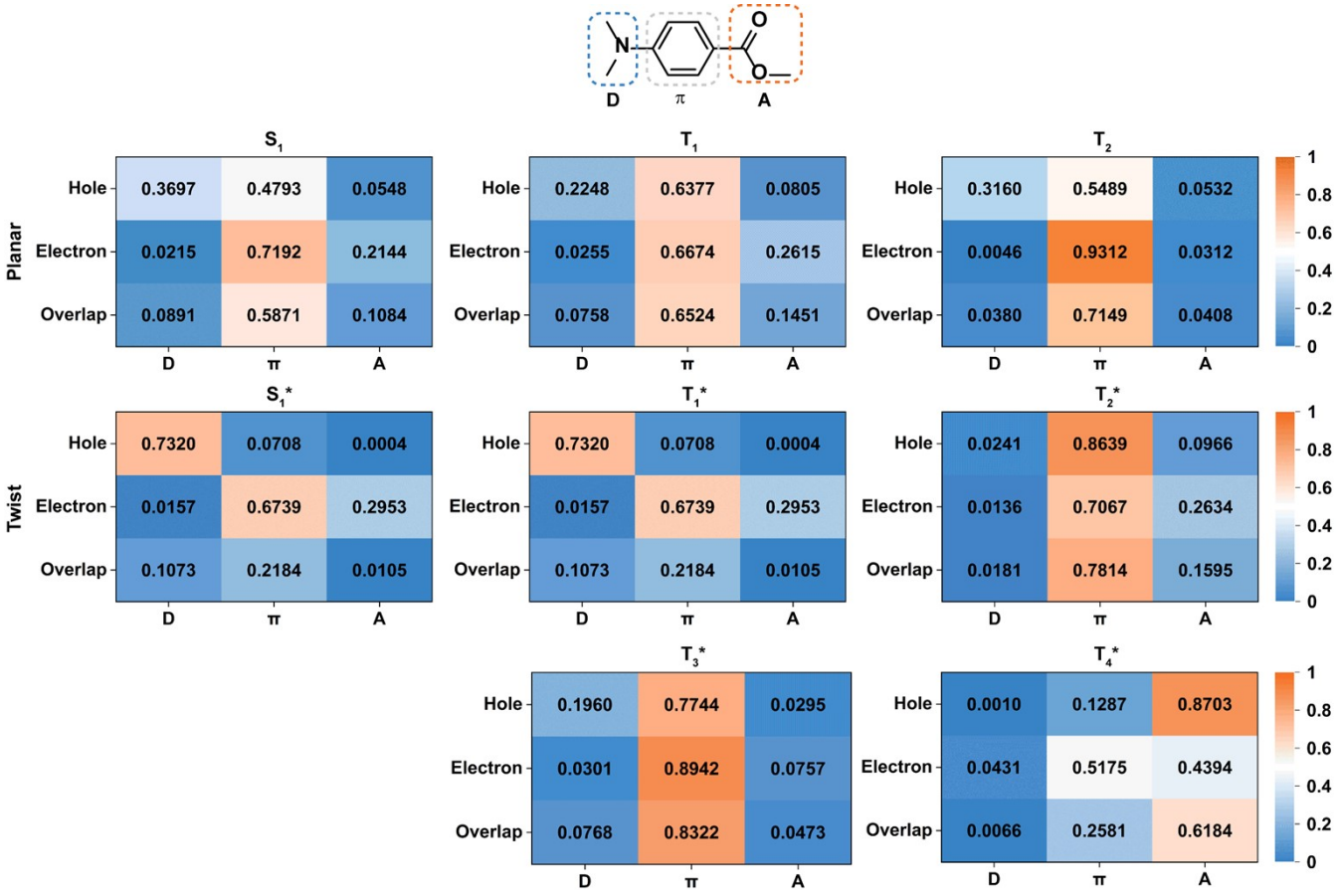

Fig. S31 The heat map of electron and hole contributions from different fragments (D, π, and A) of different excited states in the planar and twisted geometries of **N-COOMe**.

Table S10 The singlet and triplet excited state transition configurations of **N-CHO** revealed by TD-DFT calculations.

	n-th	Energy [eV]	Wavelength [nm]	f	Transition configuration
S_n	1	3.2399	382.68	0.0001	H-1 → L 96.0%
	2	4.1756	296.92	0.5726	H → L 95.9%
T_n	1	2.4354	509.09	--	H → L 91.7%, H-3 → L 6.8%
	2	2.6695	464.45	--	H-1 → L 93.1%, H-1 → L+3 6.7%
	3	3.9551	313.48	--	H → L+1 92.8%
	4	4.1067	301.91	--	H-2 → L 35.5%, H-2 → L+1 31.6%, H-3 → L 18.9%
S_n*	1	3.1090	398.79	0.0001	H-1 → L 95.7%
	2	3.4353	360.92	0.0056	H → L 97.4%
T_n*	1	2.5143	493.12	--	H-1 → L 92.9%, H-1 → L+2 6.8%
	2	2.6247	472.37	--	H-2 → L 87.2%, H-3 → L+1 6.0%
	3	3.3918	365.54	--	H → L 93.1%
	4	3.8212	324.46	--	H-3 → L 96.1%

Table S11 The singlet and triplet excited state transition configurations of **N-CO** revealed by TD-DFT calculations.

	n-th	Energy [eV]	Wavelength [nm]	f	Transition configuration
S_n	1	3.1904	388.61	0.0001	H-1 → L 96.1%
	2	4.1793	296.66	0.5903	H → L 97.1%
T_n	1	2.4968	496.57	--	H → L 91.1%, H-3 → L 7.1%
	2	2.6539	467.17	--	H-1 → L 93.2%, H-1→ L+4 6.4%
	3	3.9493	313.94	--	H → L+1 95.5%
	4	4.1324	300.03	--	H-3 → L 30.4%, H-2 → L 26.4%, H-2 → L+1 26.3%, H → L 7.0%
S_n*	1	3.0089	412.05	0.0000	H-1 → L 93.9%
	2	3.5027	353.97	0.0067	H → L 95.5%
T_n*	1	2.4647	503.04	--	H-1 → L 92.1%, H-1 → L+2 5.9%
	2	2.6416	469.35	--	H-2 → L 86.2%, H-3 → L+1 5.8%
	3	3.4573	358.62	--	H → L 91.7%
	4	3.8563	321.51	--	H-3 → L 95.8%

Table S12 The singlet and triplet excited state transition configurations of **N-COOMe** revealed by TD-DFT calculations.

	n-th	Energy [eV]	Wavelength [nm]	f	Transition configuration
S_n	1	4.1089	301.75	0.3636	H → L 91.2%, H → L+1 6.2%
	2	4.5719	271.19	0.1096	H → L+1 75.6%, H-1 → L 16.8%, H → L 6.2%
T_n	1	2.7250	454.99	--	H → L 89.0%
	2	3.8384	323.01	--	H → L+1 88.5%, H-1 → L+1 5.2%
	3	4.1725	297.15	--	H-3 → L 55.0%, H-4 → L 22.3%, H → L+3 5.5%
	4	4.4687	277.45	--	H-4 → L 53.0%, H-3 → L 27.8%
	5	4.5679	271.42	--	H-1 → L 46.9%, H-1 → L+1 33.8%, H-2 → L 8.2%
S_n*	1	2.7719	447.29	0.0000	H → L 98.2%
	2	4.0793	303.94	0.0001	H → L+1 99.8%
T_n*	1	2.7405	452.41	--	H → L 98.0%
	2	3.0328	408.81	--	H-1 → L 88.3%, H-2 → L+1 10.5%
	3	4.1725	297.15	--	H → L+1 99.6%
	4	4.4687	277.45	--	H-2 → L 95.9%

Table S13 Calculated configuration proportion α_n of different excited state in planar geometries for **N-CHO** based on MPA.

	Basic Type	Atom	Composition	α_n
S_1/ H-1	X	8(O)	15.52425 %	$\alpha_O = 77.11\% \times 96.0\% = 74.02\%$
	Y	8(O)	16.87032 %	
	X	8(O)	14.78178 %	
	Y	8(O)	15.42795 %	
	X	8(O)	7.54930 %	
	Y	8(O)	6.95538 %	
T_1/ H	Z	8(O)	4.87821 %	$\alpha_O = 0\%$
	Z	8(O)	4.54047 %	
	Z	8(O)	2.27276 %	
	Z	9(N)	12.49944 %	
	Z	9(N)	11.40039 %	
	Z	9(N)	3.05143 %	
T_1/ H-3	Z	8(O)	8.35617 %	
	Z	8(O)	8.52552 %	
	Z	8(O)	4.45358 %	
	Z	9(N)	8.35117 %	
	Z	9(N)	8.35879 %	
	Z	9(N)	3.45744 %	
T_2/ H-1	X	8(O)	15.52425 %	$\alpha_O = 77.11\% \times 99.80\% = 76.95\%$
	Y	8(O)	16.87032 %	
	X	8(O)	14.78178 %	
	Y	8(O)	15.42795 %	
	X	8(O)	7.54930 %	
	Y	8(O)	6.95538 %	
T_3/ H	Z	8(O)	4.87821 %	$\alpha_O = 0\%$
	Z	8(O)	4.54047 %	
	Z	8(O)	2.27276 %	
	Z	9(N)	12.49944 %	
	Z	9(N)	11.40039 %	
	Z	9(N)	3.05143 %	
T_4/ H-3	Z	8(O)	8.35617 %	$\alpha_O = 0\%$
	Z	8(O)	8.52552 %	
	Z	8(O)	4.45358 %	
	Z	9(N)	8.35117 %	
	Z	9(N)	8.35879 %	
	Z	9(N)	3.45744 %	
T_4/ H-2	--	--	--	

Table S14 Calculated configuration proportion α_n of different excited state in twisted geometries for **N-CHO** based on MPA.

	Basic Type	Atom	Composition	α_n
S_1*/ H-1	X	8(O)	12.70425 %	$\alpha_O = 75.30\% \times 95.7\% = 72.06\%$
	Y	8(O)	19.19671 %	
	X	8(O)	12.10607 %	
	Y	8(O)	17.49378 %	
	X	8(O)	6.10696 %	
	Y	8(O)	7.69304 %	
T_1*/ H-1	X	8(O)	12.70425 %	$\alpha_O = 75.30\% \times 99.7\% = 75.07\%$
	Y	8(O)	19.19671 %	
	X	8(O)	12.10607 %	
	Y	8(O)	17.49378 %	
	X	8(O)	6.10696 %	
	Y	8(O)	7.69304 %	
T_2*/ H-2	Z	8(O)	7.45837 %	$\alpha_O = 0\%$
	Z	8(O)	7.19784 %	
	Z	8(O)	3.49115 %	
T_2*/ H-3	Z	8(O)	0%	
T3*/ H	Y	9(N)	23.88431 %	$\alpha_N = 57.65\% \times 93.1\% = 53.67\%$
	Z	9(N)	0.75786 %	
	Y	9(N)	22.90849 %	
	Z	9(N)	0.71021 %	
	Y	9(N)	10.85537 %	
T_4*/ H-3	Z	8(O)	0%	$\alpha_O = 0\%$

Table S15 Calculated configuration proportion α_n of different excited state in planar geometries for **N-CO** based on MPA.

	Basic Type	Atom	Composition	α_n
S_1/ H-1	X	8(O)	20.47299 %	$\alpha_O = 76.87\% \times 96.1\% = 73.87\%$
	Y	8(O)	11.90359 %	
	X	8(O)	19.25791 %	
	Y	8(O)	10.73581 %	
	X	8(O)	9.77214 %	
	Y	8(O)	4.72283 %	
T_1/ H	Z	8(O)	4.55938 %	$\alpha_O = 0\%$
	Z	8(O)	4.26602 %	
	Z	8(O)	2.19064 %	
	Z	9(N)	12.56035 %	
	Z	9(N)	11.45220 %	
	Z	9(N)	3.07459 %	
T_1/ H-3	Z	8(O)	10.01865 %	
	Z	8(O)	10.24444 %	
	Z	8(O)	5.46069 %	
	Z	9(N)	7.69123 %	
	Z	9(N)	7.68877 %	
	Z	9(N)	3.16527 %	
T_2/ H-1	X	8(O)	20.47299 %	$\alpha_O = 76.87\% \times 99.8\% = 76.72\%$
	Y	8(O)	11.90359 %	
	X	8(O)	19.25791 %	
	Y	8(O)	10.73581 %	
	X	8(O)	9.77214 %	
	Y	8(O)	4.72283 %	
T_3/ H	Z	8(O)	4.55938 %	$\alpha_O = 0\%$
	Z	8(O)	4.26602 %	
	Z	8(O)	2.19064 %	
	Z	9(N)	12.56035 %	
	Z	9(N)	11.45220 %	
	Z	9(N)	3.07459 %	
T_4/ H	Z	8(O)	4.55938 %	$\alpha_O = 0\%$
	Z	8(O)	4.26602 %	
	Z	8(O)	2.19064 %	
	Z	9(N)	12.56035 %	
	Z	9(N)	11.45220 %	
	Z	9(N)	3.07459 %	
T_4/ H-2	--	--	--	
T_4/ H-3	Z	8(O)	10.01865 %	
	Z	8(O)	10.24444 %	

	Z	8(O)	5.46069 %
	Z	9(N)	7.69123 %
	Z	9(N)	7.68877 %
	Z	9(N)	3.16527 %

Table S16 Calculated configuration proportion α_n of different excited state in twisted geometries for **N-CO** based on MPA.

	Basic Type	Atom	Composition	α_n
S_1*/ H-1	X	8(O)	18.60534 %	$\alpha_O = 74.58\% \times 93.9\% = 70.04\%$
	Y	8(O)	12.82579 %	
	X	8(O)	17.46883 %	
	Y	8(O)	11.51121 %	
	X	8(O)	9.04326 %	
	Y	8(O)	5.13115 %	
T_1*/ H-1	X	8(O)	18.60534 %	$\alpha_O = 74.58\% \times 98.00\% = 73.09\%$
	Y	8(O)	12.82579 %	
	X	8(O)	17.46883 %	
	Y	8(O)	11.51121 %	
	X	8(O)	9.04326 %	
	Y	8(O)	5.13115 %	
T_2*/ H-2	Z	8(O)	7.89519 %	$\alpha_O = 0\%$
	Z	8(O)	7.68163 %	
	Z	8(O)	3.73457 %	
T_2*/ H-3	Z	8(O)	0%	
T_3*/ H	X	9(N)	0.86178 %	$\alpha_N = 57.73\% \times 91.7\% = 52.94\%$
	Y	9(N)	23.25557 %	
	X	9(N)	0.75969 %	
	Y	9(N)	22.32265 %	
	Y	9(N)	10.53145 %	
T_4*/ H-3	Z	8(O)	0%	$\alpha_O = 0\%$

Table S17 Calculated configuration proportion α_n of different excited state in planar geometries for **N-COOMe** based on MPA.

	Basic Type	Atom	Composition	α_n
S_1/ H	Z	8(O)	1.56405 %	$\alpha_O = 0\%$ $\alpha_N = 3.10\% \times 97.4\% = 3.02\%$
	Z	8(O)	1.40485 %	
	Z	8(O)	0.53749 %	
	Y	9(N)	1.28549 %	
	Z	9(N)	13.37345 %	
	Y	9(N)	1.21164 %	
	Z	9(N)	12.19201 %	
	Y	9(N)	0.60766 %	
	Z	9(N)	3.64612 %	
T_1/ H	Z	8(O)	1.56405 %	$\alpha_O = 0\%$ $\alpha_N = 3.10\% \times 89.0\% = 2.76\%$
	Z	8(O)	1.40485 %	
	Z	8(O)	0.53749 %	
	Y	9(N)	1.28549 %	
	Z	9(N)	13.37345 %	
	Y	9(N)	1.21164 %	
	Z	9(N)	12.19201 %	
	Y	9(N)	0.60766 %	
	Z	9(N)	3.64612 %	
T_2/ H	Z	8(O)	1.56405 %	$\alpha_O = 0\%$ $\alpha_N = 3.10\% \times 88.5\% = 2.75\%$
	Z	8(O)	1.40485 %	
	Z	8(O)	0.53749 %	
	Y	9(N)	1.28549 %	
	Z	9(N)	13.37345 %	
	Y	9(N)	1.21164 %	
	Z	9(N)	12.19201 %	
	Y	9(N)	0.60766 %	
	Z	9(N)	3.64612 %	
T_3/ H-3	Z	8(O)	3.07864 %	$\alpha_O = 0\%$ $\alpha_N = 2.55\% \times 55.0\% + 3.10\% \times 5.0\% = 1.56\%$
	Z	8(O)	2.99843 %	
	Z	8(O)	1.30714 %	
	Y	9(N)	1.33607 %	
	Z	9(N)	6.53685 %	
	Y	9(N)	1.21380 %	
	Z	9(N)	6.76332 %	
	Z	9(N)	3.35588 %	
T_3/ H-4	Z	8(O)	10.40268 %	
	Z	8(O)	10.24390 %	
	Z	8(O)	5.66254 %	
	Z	12(O)	20.94740 %	

	Z	12(O)	19.19556 %	
	Z	12(O)	7.44950 %	
T_3/ H	Z	8(O)	1.56405 %	
	Z	8(O)	1.40485 %	
	Z	8(O)	0.53749 %	
	Y	9(N)	1.28549 %	
	Z	9(N)	13.37345 %	
	Y	9(N)	1.21164 %	
	Z	9(N)	12.19201 %	
	Y	9(N)	0.60766 %	
	Z	9(N)	3.64612 %	
T_4/ H-3	Z	8(O)	3.07864 %	$\alpha_O = 0\%$ $\alpha_N = 2.55\% \times 27.8\% = 0.71\%$
	Z	8(O)	2.99843 %	
	Z	8(O)	1.30714 %	
	Y	9(N)	1.33607 %	
	Z	9(N)	6.53685 %	
	Y	9(N)	1.21380 %	
	Z	9(N)	6.76332 %	
	Z	9(N)	3.35588 %	
T_4/ H-4	Z	8(O)	10.40268 %	
	Z	8(O)	10.24390 %	
	Z	8(O)	5.66254 %	
	Z	12(O)	20.94740 %	
	Z	12(O)	19.19556 %	
	Z	12(O)	7.44950 %	

Table S18 Calculated configuration proportion α_n of different excited state in twisted geometries for **N-COOMe** based on MPA.

	Basic Type	Atom	Composition	α_n
S_1*/ H	Y	9(N)	27.01823 %	$\alpha_N = 63.55\% \times 98.2\% = 62.41\%$
	Y	9(N)	25.22026 %	
	Y	9(N)	11.31411 %	
T_1*/ H	Y	9(N)	27.01823 %	$\alpha_N = 63.55\% \times 98.0\% = 62.28\%$
	Y	9(N)	25.22026 %	
	Y	9(N)	11.31411 %	
T_2*/ H-1	Z	8(O)	3.16681 %	$\alpha_O = 0\%$
	Z	8(O)	2.98432 %	
	Z	8(O)	1.20665 %	
	Z	12(O)	0.88727 %	
	Z	12(O)	0.76838 %	
T_3*/ H	Y	9(N)	27.01823 %	$\alpha_N = 63.55\% \times 99.6\% = 63.3\%$
	Y	9(N)	25.22026 %	
	Y	9(N)	11.31411 %	
T_4*/ H-2	--	--	--	$\alpha_N = 0\%$

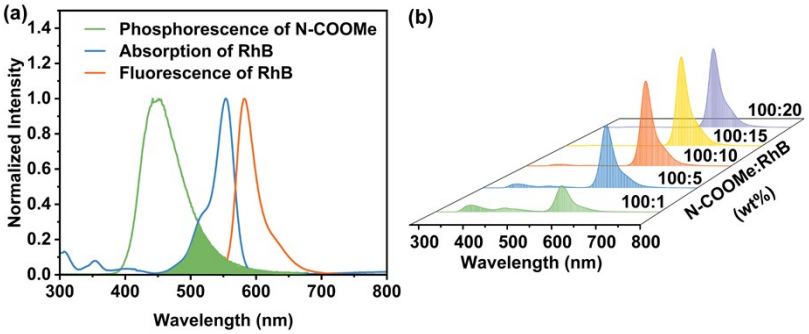

Fig. S32 (a) The normalized phosphorescence spectra of **N-COOMe** doped PVA film, aa well as the normalized absorption and fluorescence spectra of **RhB** aqueous solution, $C = 5\times10^{-5}$ mol/L. (b) The fluorescence spectra of the hybrid film with different ratio of donor and acceptor.

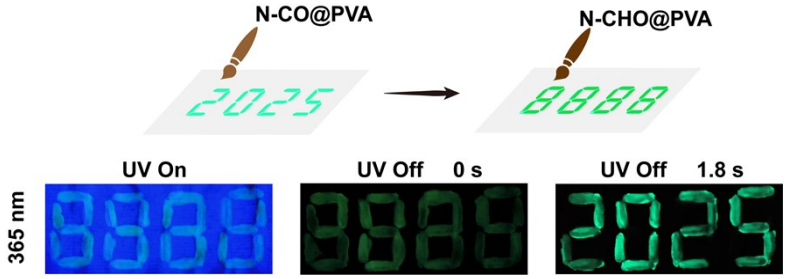

Fig. S33 Processes of encrypted information writing by using **N-CO@PVA** and **N-CHO@PVA**, as well as and photographs of time-dependent information security encryption.

4. Reference

1. Z. Yin, M. Gu, H. Ma, X. Jiang, J. Zhi, Y. Wang, H. Yang, W. Zhu and Z. An, Angew. Chem. Int. Ed., 2021, 60, 2058-2063.
2. W. Humphrey, A. Dalke and K. Schulten, J. Mol. Graph., 1996, 14, 33-38.
3. T. Lu and F. Chen, J. Comput. Chem., 2012, 33, 580-592.
4. Z. Liu, T. Lu and Q. Chen, Carbon, 2020, 165, 461-467.
5. W. J. Zhao, Z. K. He, J. W. Y. Lam, Q. Peng, H. L. Ma, Z. G. Shuai, G. X. Bai, J. H. Hao and B. Z. Tang, Chem, 2016, 1, 592-602.
6. H. Ma, Q. Peng, Z. An, W. Huang and Z. Shuai, J. Am. Chem. Soc., 2018, 141, 1010-1015.
7. F. Neese, F. Wennmohs, U. Becker and C. Riplinger, J. Chem. Phys., 2020, 152, 224108.
8. F. Neese, WIREs Comput. Mol. Sci. , 2018, 8, e1327.
9. F. Neese, WIREs Comput. Mol. Sci. , 2012, 2, 73-78.
10. D. Cui, L. Zhang, J. Zhang, W. Li, J. Chen, Z. Guo, C. Sun, Y. Wang, W. Wang, S. Li, W. Huang, C. Zheng and R. Chen, Angew. Chem. Int. Ed., 2024, 63, e202411588.
11. J. E. Leffler and E. Grunwald, *Rates and Equilibria of Organic Reactions*, Wiley, New York, 1963.